AD-A040 397 HARRY DIAMOND LABS ADELPHI MD F/G 17/5
RESPONSE OF LWIR HGCDTE PHOTOCONDUCTIVE DETECTORS TO IONIZING R--ETC(U)
DEC 76 S SHARE
UNCLASSIFIED HDL-TR-1768 NL

| OF |
AD
A040 397

END

DATE
FILMED
6-77

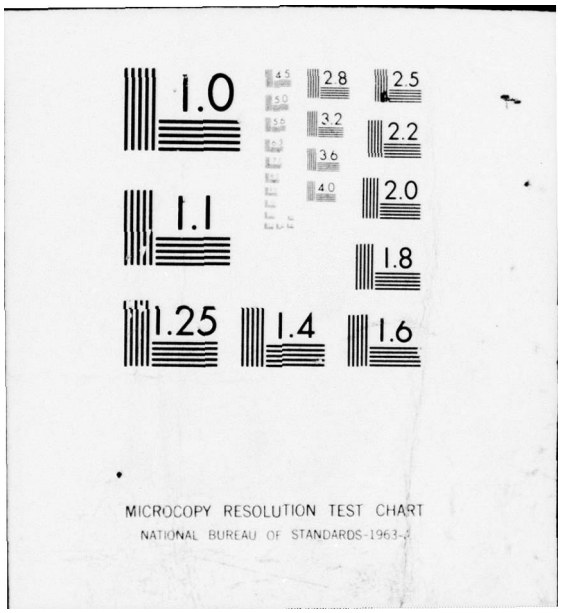
1.0
1.1
1.25
1.4
1.6
1.8
2.0
2.2
2.5
2.8
3.2
3.6
4.0
4.5
5.0
5.6
6.3
7.1
8.0
9.0
MICROCOPY RESOLUTION TEST CHART
NATIONAL BUREAU OF STANDARDS-1963-A

HDL-TR-1768

Response of LWIR HgCdTe Photoconductive Detectors to Ionizing Radiation

December 1976

U.S. Army Materiel Development and Readiness Command
HARRY DIAMOND LABORATORIES
Adelphi, Maryland 20783

The findings in this report are not to be construed as an official Department of the Army position unless so designated by other authorized documents.

Citation of manufacturers' or trade names does not constitute an official indorsement or approval of the use thereof.

Destroy this report when it is no longer needed. Do not return it to the originator.

UNCLASSIFIED

SECURITY CLASSIFICATION OF THIS PAGE *(When Data Entered)*

REPORT DOCUMENTATION PAGE

READ INSTRUCTIONS BEFORE COMPLETING FORM

1. REPORT NUMBER: HDL-TR-1768	2. GOVT ACCESSION NO.
3. RECIPIENT'S CATALOG NUMBER	
4. TITLE *(and Subtitle)*: Response of LWIR HgCdTe Photoconductive Detectors to Ionizing Radiation.	5. TYPE OF REPORT & PERIOD COVERED: Technical Report.
	6. PERFORMING ORG. REPORT NUMBER
7. AUTHOR(s): Stewart Share	8. CONTRACT OR GRANT NUMBER(s): DA: 8X363304D215
9. PERFORMING ORGANIZATION NAME AND ADDRESS: Harry Diamond Laboratories, 2800 Powder Mill Road, Adelphi, MD 20783	10. PROGRAM ELEMENT, PROJECT, TASK AREA & WORK UNIT NUMBERS: Program Element: 6.33.04.A
11. CONTROLLING OFFICE NAME AND ADDRESS: Ballistic Missile Defense, Advanced Technology Center, Huntsville, AL 35807	12. REPORT DATE: December 1976
	13. NUMBER OF PAGES: 54
14. MONITORING AGENCY NAME & ADDRESS *(if different from Controlling Office)*: 12 47p.	15. SECURITY CLASS. *(of this report)*: UNCLASSIFIED
	15a. DECLASSIFICATION/DOWNGRADING SCHEDULE

16. DISTRIBUTION STATEMENT *(of this Report)*

Approved for public release; distribution unlimited.

17. DISTRIBUTION STATEMENT *(of the abstract entered in Block 20, if different from Report)*

18. SUPPLEMENTARY NOTES

HDL Project: 224628
DRCMS Code 697000.22.11551

19. KEY WORDS *(Continue on reverse side if necessary and identify by block number)*

Radiation effects
HgCdTe
Photoconductive detectors

20. ABSTRACT *(Continue on reverse side if necessary and identify by block number)*

The effect of ionizing radiation on 0.09-eV bandgap long wavelength infrared HgCdTe photoconductive detectors at 77°K has been investigated. The results of pulsed gamma, gamma-counting, and gamma-induced noise experiments indicate that the average value of the electron-hole pair creation energy, ϵ_p of $Hg_{0.8}Cd_{0.2}Te$ is 0.36 ± 0.07 eV. Analysis of gamma-counting and gamma-induced noise experiments indicate that the majority of the gamma events

DD FORM 1 JAN 73 1473 EDITION OF 1 NOV 65 IS OBSOLETE

UNCLASSIFIED

SECURITY CLASSIFICATION OF THIS PAGE *(When Data Entered)*

163 050

originate from Compton interactions in the surrounding material--for example, glass dewar external to the detector. Initial decay characteristics of the detector response following a prompt gamma pulse appear to depend on the detector material, proceeding either through a bimolecular or a Shockley-Read recombination process. At longer times following the pulse, trap-limited processes become operative in which the fractional level of decay eventually reaches the same value for all the material-preparation techniques evaluated in this work. This applies to detectors in which the surface was left untreated, or was passivated. A detector with the surface treated with a ZnS antireflection coating, however, exhibited an enhanced long time decay response at the largest gamma doses.

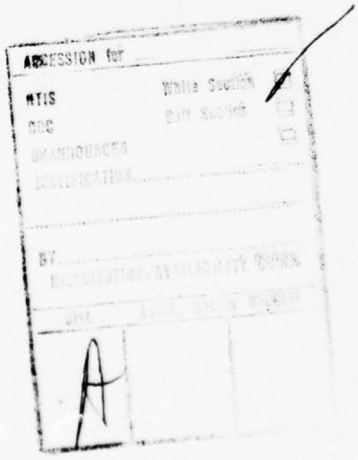

CONTENTS

FIGURES

FIGURES (CONT'D)

FIGURES (CONT'D)

TABLES

1. INTRODUCTION

Infrared sensing elements are being used or are under consideration for use in a wide variety of system applications including guidance, fuzing, and surveillance. In addition to being sensitive to optical radiation, they are also expected to be sensitive to high-energy ionizing radiation, such as would be encountered in a hostile nuclear environment. Because many systems are required to maintain operation in such environments, it is necessary to know and to be able to predict the effect of nuclear radiation on optical detectors.

This report discusses the effect of ionizing radiation on long wavelength infrared (LWIR) HgCdTe photoconductive optical detectors. A variety of effects, detrimental to system operation, can result when the detector is placed in such an environment. From a system standpoint, for example, a low-level background can produce false signals which, in turn, can result in a system misfiring, a high-level background can degrade system sensitivity below specification, and a transient pulse can cause the system to be "off the air" for an extended time interval. These effects will be modeled and then applied to experimental data taken on representative commercial HgCdTe devices.

2. FACILITIES

The low- and high-level radiation background experiments were performed at the 39 kCi ^{60}Co air source located at the Armed Forces Radiobiological Research Institute. By varying the distance between the source and the detector, gamma fields were obtained with dose rates ranging from 1 to 220 rads/s at the detector. The dose rate was measured actively with an air ionization chamber and a digital readout.

Transient pulse experiments--that is, prompt gamma--were performed at the High Intensity Flash X-Ray (HIFX) located at the Harry Diamond Laboratories. Dosimetry was accomplished by CaF thermoluminescent dosimeters (TLD's) and a Victoreen TLD reader. The width (FWHM) of the x-ray pulse is 21 ns; the energy spectrum peaks at 2 MeV. Total dose ranged from 0.2 to 360 rads, depending on the distance between the Ta bremsstrahlung target and the detector.

3. PREIRRADIATION DEVICE DATA

Four different detectors were studied. Two of them were supplied by Honeywell Radiation Center and denoted HRC and HRC #8, one was supplied by Arthur D. Little, Inc. and denoted ADL, and one was supplied by Aeronutronic Ford Corp. and denoted AF.

Table I lists several device parameters, including device area (A), device thickness (d), extrinsic carrier concentration (n_o), detector resistance between the contacts (R), peak detector responsivity (R_λ) at 12-μm wavelength at a bias (V_B), and the condition of the surface. All the samples were n-type. The carrier concentrations are known to approximately ±20 percent, except for the ADL device which is known only approximately within a factor of 2. All the detector areas were square,

TABLE I. PHOTODETECTOR DATA

Detector	A (cm^2)	d (cm)	n_o (cm^{-3})	R (Ω)	$R_\lambda \mid V_B$ (V/W|V)	Surface
HRC	10^{-5}	1.2×10^{-3}	7×10^{14}	54	1.3×10^{5}|.11	ZnS
ADL	6.25×10^{-4}	1.2×10^{-3}	2.5×10^{14}	140	840|.14	Untreated
AF	4.5×10^{-3}	2.5×10^{-3}	8.0×10^{14}	90	750|.45	Pass
HRC #8	6.25×10^{-4}	1.2×10^{-3}	10^{15}	25	1800|.25	Untreated

except for the AF device which was 0.175 by 0.025 cm. The detectors were mounted in LN_2 dewars enabling them to be operated at 77°K. All the detectors were designed to have a wavelength cutoff of λ_{co} = 13 to 14 μm, which is equivalent to an alloy concentration of approximately 20 percent Cd, that is, $Hg_{0.80}Cd_{0.20}Te$.

The AF detector material used for fabricating the units was supplied by Cominco, Inc. The material was grown by a process similar to the slush-recrystallization technique developed by Harman.[1] The detector was epoxy-mounted on a sapphire substrate which was, in turn, epoxy-mounted on a No. 42 alloy. A passivation coating was deposited over the detector. There was no ZnS antireflection coating. The dewar window was Ge with an antireflection coating. The ADL detector material was grown in a high-pressure furnace[2] by an open ampoule technique that allowed impurities--for example, Cl, O, N, and H--to boil off. The detector was mounted on an IRTRAN II substrate (ZnS) and was in optical contact (that is, not air spaced) to a Ge immersion lens. The dewar window was IRTRAN II. The detector surface was untreated--that is, no passivation or ZnS antireflection coating. The Honeywell detectors were grown in a Bridgeman Furnace[3] by a closed ampoule technique. Two detectors were studied. One (HRC) was mounted on a ZnS substrate and had a ZnS antireflective coating on the detector and an IRTRAN II dewar window. The other was mounted on a sapphire substrate and also had a Ge dewar window. The detector surface was left untreated.

---

[1] *T. C. Harman, J. Electronic Mat., 1, (1972). p. 230.*

[2] *J. Steininger, Proceedings of Meeting of IRIS Specialty Group on IR Detectors (13-15 March 1973) p. 33.*

[3] *P. W. Kruse, Appl. Optics, 4 (1965), p. 687.*

4. EXPERIMENTAL PROCEDURE

Following a prompt gamma pulse, the recovery of the detector was recorded with a Tektronix 7844 oscilloscope and 7A13 and 7A22 differential plug-ins. The peak of the response was measured by the 7A13 plug-in with a 5-MHz bandwidth. The decay of the response was obtained by using the 7A22 with a high-frequency cutoff set at 1 MHz and a low-frequency cutoff set at 1 Hz. This plug-in has a 15-V overload capability down to the lowest gain sensitives used (1 mV/cm) with overload recovery of the plug-in rated at less than 10 μs. For the maximum voltages (peak) measured on this experiment (~200 mV), the plug-in was not driven into saturation. Figure 1 shows the bias circuit. To reduce the rf pickup from the HIFX pulse so that measurements could be made at times immediately following the pulse, it was necessary to double shield the detector and all leads in addition to using the differential plug-in. The oscilloscope, which was terminated at 50 Ω, and the bias battery were housed in a metal (shielding) box located outside the exposure room. The bias circuit was placed in close proximity to the detector.

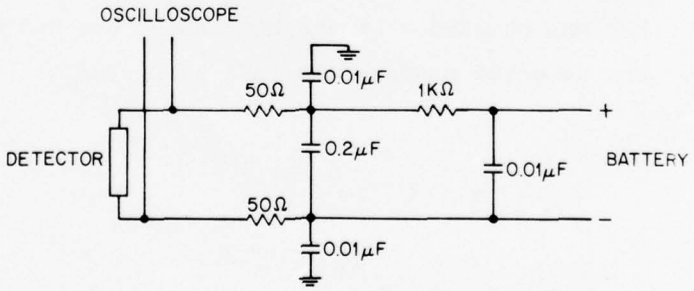

Figure 1. HIFX bias circuit.

The high-level gamma-induced noise measurements were obtained with a Ballentine 320A rms voltmeter, using a 4-MHz bandwidth followed by a 10-MHz-bandwidth amplifier with a gain of 200 placed at the detector input. The detector and amplifier were located in the exposure room and were separated from the measuring apparatus by 30 m. Connections were made with RG-178 cable. The amplifier circuit shown in figure 2 includes a biasing circuit designed to operate at 3-mA detector current.

By replacing the rms voltmeter with a Tektronix 454 oscilloscope and an Ortec counter/scaler, the low-level gamma counting measurements were performed. By using the internal trigger level control, the oscilloscope served as a voltage discriminator. Gamma-induced detector voltage pulses with amplitudes greater than the discrimination level are counted on the counter/scaler via the gate output of the oscilloscope. In this way, the pulse height distribution of the detector noise could be determined.

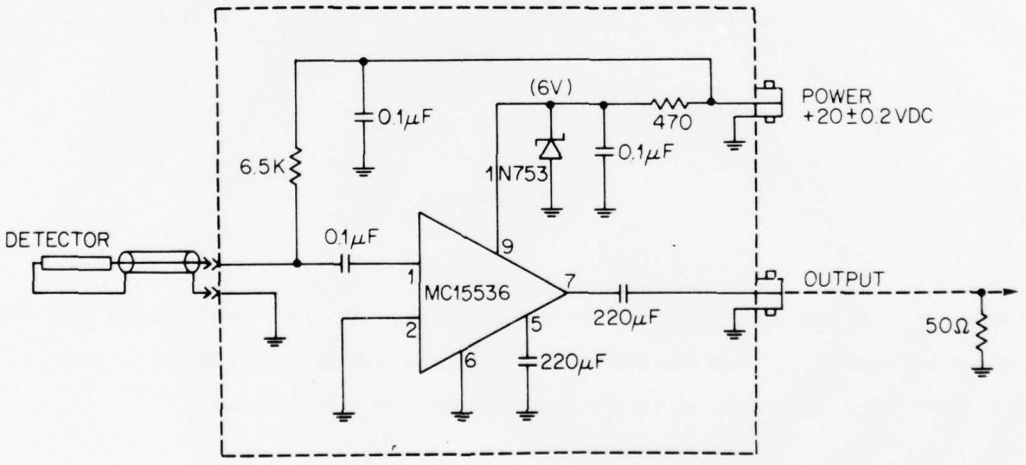

Figure 2. Schematic diagram of 10-MHz preamplifier.

5. THEORY

5.1 Prompt Gamma Pulse

High-energy ionizing radiation incident on a photoconductor generates electron-hole pairs. These give rise to a short circuit photocurrent which can be written as

$$I_s = q\mu V_B \Delta N/\ell^2 \ . \tag{1}$$

In this equation, q is the charge of an electron, μ is the carrier mobility, V_B is the voltage across the detector, ΔN is the number of carriers generated by the incident radiation, and ℓ is the distance between the current-carrying electrodes. When the load resistor R_L in the bias circuit is greater than detector resistance R_d, the open-circuit voltage V is measured at the detector electrodes; V is given by

$$V = I_s R_d \ . \tag{2}$$

The detector resistance is given by

$$R_d = \ell/wdq\mu n_o \ , \tag{3}$$

where n_o is the extrinsic carrier density, w is the width of the detector, and d is the thickness of the detector. From equations (1), (2), and (3), the open-circuit voltage may be written as

$$V = V_B \Delta n/n \ , \tag{4}$$

where Δn is the density (cm^{-3}) of excess carrier ($\Delta n = \Delta N/w\ell d$) induced by the radiation. The biasing circuits in this experiment (fig. 1 and 2) utilize large load resistors $R_L >> R_D$; thus, the detector voltage induced by the ionizing radiation is given by equation (4).

In equation (4), Δn is written as

$$\Delta n = 100\rho\dot{D}\tau/\varepsilon_\rho \ , \tag{5}$$

where ρ is the density of the $Hg_{0.8}Cd_{0.2}Te$, $\dot{D}$ is the dose rate in rad/s, τ is the lifetime of the excess carriers, and ε_ρ is the electron-hole pair creation energy (in ergs). This expression is valid when the gamma-pulse width is longer than the lifetime. When the lifetime is longer than or equal to the pulse width, equation (5) may be written as

$$\Delta n = 100\rho D/\varepsilon_\rho \ , \tag{6}$$

where D is the dose in the HgCdTe. The value of Δn in equation (6) is for times immediately following the ionizing pulse. At later times, t, after the pulse, the excess carriers decay, to a first approximation, through a single exponential time constant (τ); Δn is given by

$$\Delta n = \left(100\rho De^{-t/\tau}\right)/\varepsilon_\rho . \tag{7}$$

For low-radiation levels (in equation (4)), n is the initial (electron) doping concentration n_o. As the radiation level increases, the excess carrier concentration Δn becomes comparable in magnitude with n_o, so that n is written as $n_o + \Delta n$. Substituting this in equation (4) yields

$$V = V_B\Delta n/\left(n_o + \Delta n\right) . \tag{8}$$

From this equation, the detector voltage resulting from an ionizing radiation pulse (induced by the irradiation) saturates at the detector bias voltage. Equations (7) and (8) will be used to analyze the peak detector voltages induced by the prompt gamma pulse.

5.2 Low-Level Gamma Counting

The effect of a high fluence density of ionizing radiation on HgCdTe detectors has been presented in the preceding section. This section considers the effect of individual high-energy gamma photons on the detector.

High-energy photons, such as would be emitted from a ^{60}Co source (1.17 and 1.32 MeV), interact with the detector primarily through secondary Compton electrons that are emitted from collisions of the gammas with material (i.e., glass) surrounding the detector.[4,5] Passage of the electron through the detector ionizes electron-hole pairs and gives rise to a voltage pulse at the detector. An approximate value of the voltage pulse induced in the detector[6] is, from equation (4),

$$V_P = V_B N_\gamma / w\ell dn_o \ , \qquad (9)$$

where N_γ is the number of electron-hole pairs released by the passage of a Compton electron. Assuming that these electrons pass through the thickness (d) of the detector, N_γ may be approximated by

---

[4] *R. A. Rotolante, R. P. Muroska, and G. E. Keiser, Radiation Effects in Intrinsic Photodetector Systems (U), Honeywell Radiation Center AMMRC CTR 73-46 (December 1973). (SECRET)*

[5] *J. W. Haffner, Presented at 1975 IEEE, Annual Conference Nuclear and Space Radiation Effects, Poster Session Paper (14-17 July 1975).*

[6] *Detector Test Program Final Report, Vol. 1, LMSC-B303910, Contract F04701-70-C-0227 (August 1972).*

$$N_\gamma = \frac{dE}{dx}\frac{d}{\varepsilon_\rho}, \tag{10}$$

where dE/dx is the ionization loss rate of the high-energy electrons. A value of N_γ, corresponding to passage through the length (ℓ) and width (w), can be obtained by the appropriate substitutions. However, the probability for such an event is small compared with passage through the thickness.

Calculation of the complete pulse-height distribution requires an involved computer formulation.[7] However, a rather good closed form expression can be obtained by considering the isotropic interaction of Compton electrons originating in the surrounding material with the detector.[5] By using an approximate expression for the Compton cross section, an expression for the number of voltage pulses per second out of the detector greater than or equal to a threshold value (P) can be written

$$\text{counts/s}(\geq P) = C_6\left\{\exp\left[-(C_2 + C_7)\sin\sqrt{1-(kd/P)^2}\right]\left[\frac{\sin\sqrt{1-(kd/P)^2}}{(C_2 + C_7)} + \frac{1}{(C_2 + C_7)^2}\right] - \exp\left[-(C_2 + C_7)\sin\theta_{max}\right]\left[\frac{\sin\theta_{max}}{C_2 + C_7} + \frac{1}{(C_2 + C_7)}\right]\right\}. \tag{11}$$

---

[5] *J. W. Haffner, Presented at 1975 IEEE, Annual Conference Nuclear and Space Radiation Effects, Poster Session Paper (14-17 July 1975).*

[7] *J. C. Pickel and M. D. Petroff, IEEE Trans. Nucl. Sci., NS-22, No. 6 (1975), p. 2456.*

The literal coefficients are

$$C_6 = 2\pi A N_1 \dot{\gamma} C_1 C_5$$

$$C_1 = 1.6E_\gamma + \frac{1.4}{E_\gamma^{0.2}} \cdot 10^{-25}$$

$$C_2 = 1 + 1.8\ E_\gamma$$

$$C_5 = \gamma_1 \left(\frac{E_\gamma^2}{0.25 + E_\gamma} \right)^{n_1}$$

$$C_7 = 6 \times 10^{-3} \left(2 + E_\gamma \right)^{n_1}$$

$$k = V_B \left(\frac{dE}{dx} \right) / \varepsilon_\rho n_o \ell w d$$

$$\theta_{max} = \cos^{-1} \left[\frac{d}{\delta_1} \left(\frac{E_\gamma - 1.02}{2} \right)^{-n_1} \right]$$

where

A = detector area,

N_1 = density of electrons in the surrounding cover,

$\dot{\gamma}$ = incident gamma photon flux,

E_γ = 1.25 MeV (^{60}Co energy),

n_1 and δ_1 are parameters in the range-energy (R-E_e) relationship:

$$R \approx \delta_1 \left(E_e \right)^{n_1} \quad \text{where} \quad n_1 = 5/3,\ \delta_1 = 0.27 \text{ cm} .$$

The values of $C_1 = 3.3 \times 10^{-25}$ cm^2/e, $C_2 = 3.25$ cm^2/e, $C_5 = 0.27$ cm, and $C_7 = 3.25 \times 10^{-2}$ cm. This expression applies to electrons that do not stop in the detector.

5.3 High-Level Gamma Noise

An expression for the gamma-induced noise may be obtained by analogy from background-induced generation-recombination (G-R) noise and by approximating the pulse-height distribution by an exponential (consistent with observation). The rms noise voltage from the incident gammas[6] is

$$V_\gamma = 2\tau V_p \sqrt{2E_R B}$$

$$B = 1/2\pi\tau, \quad \text{if } \Delta f \leq 1/2\pi\tau \tag{12}$$

$$B = \Delta f, \quad \text{if } \Delta f > 1/2\pi\tau ,$$

where V_p is given by equation (9), Δf is the voltmeter bandwidth, and E_R is the event rate; thus,

$$E_R = K\mu\dot{\gamma}w\ell d . \tag{13}$$

In this equation, μ is the linear absorption coefficient of high-energy gammas in HgCdTe, $\dot{\gamma}$ is the incident photon flux (number of gamma photons/$cm^2 \cdot s$), ℓwd is the detector volume, and K is a constant that accounts for the effect of secondary Compton electrons whose point of origination is external to the detector. K may be calculated with some degree of accuracy as pointed out in the previous section, or it may be obtained empirically from the experimental pulse-height distribution. When K = 1, all the pulses originate from Compton events internal to the detector volume.

---

[6] *Detector Test Program Final Report, Vol. 1, LMSC-B303910, Contract F04701-70-C-0227 (August 1972).*

6. RESULTS

6.1 Prompt Gamma

6.1.1 Data

Oscillograms of detector output voltage following a prompt gamma dose in the range of 350 rads for each of the four detectors are given in figures 3 to 6. The lower trace in each figure shows the peak response on the 100-ns/cm time base. The upper trace in each figure shows the decay tail on the appropriate time base down to 2 mV/cm (1 mV/cm for HRC detector) for each detector. The vertical scale readings must be multiplied by 2 to obtain the actual detector output voltages because of 50-Ω termination.

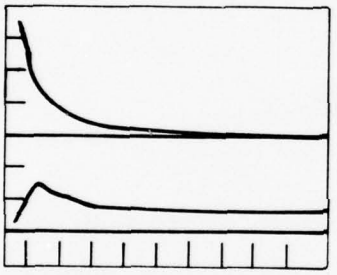

Top trace: 1 mV/cm, 500 μs/cm
Lower trace: 50 mV/cm, 100 ns/cm
V_B = 100 mV

Figure 3. Response of HRC after 350-rad HIFX prompt gamma pulse.

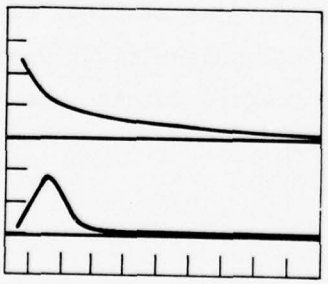

Top trace: 2 mV/cm, 5 μs/cm
Lower trace: 50 mV/cm, 100 ns/cm
V_B = 150 mV

Figure 4. Response of ADL after 340-rad HIFX prompt gamma pulse.

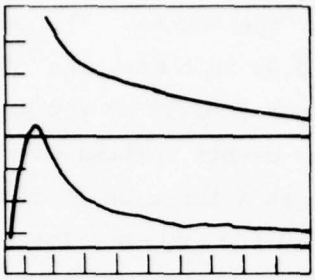

Top trace: 2 mV/cm, 1 μs/cm
Lower trace: 20 mV/cm, 100 ns/cm
V_B = 150 mV

Figure 5. Response of AF after 360-rad HIFX prompt gamma pulse.

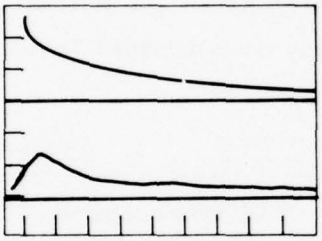

Top trace: 2 mV/cm, 2 μs/cm
Lower trace: 20 mV/cm, 100 ns/cm
V_B = 50 mV

Figure 6. Response of HRC #8 after 320-rad HIFX prompt gamma pulse.

A few interesting observations have been made about these oscillograms. First, disregarding the different detector biases, the detector designated HRC appears to have a substantially longer decay tail than that of the three other detectors. The HRC #8, AF, and ADL detectors decay to millivolts output between 10 and 20 μs after the pulse, whereas the HRC detector decays to millivolts on the order of milliseconds after the pulse. This is further demonstrated in figure 7 where V/V_B, the ratio of detector output voltage to detector bias, is plotted versus time after the gamma pulse for the various detectors. It is seen that after scaling the detector voltage by the bias voltage, the detector voltage recovered to 1 percent (0.01) of the bias voltage

at approximately 20 μs after the pulse for the HRC #8, AF, and ADL detector. The HRC detector recovered to 0.01 in 1 ms. The detector bias voltages, as seen in figure 7, ranged from 50 mV for HRC #8 to 256 mV for AF. Figure 8 gives the detector output voltage of the HRC, AF, and ADL following a 280-rad gamma dose as a function of time after the pulse. The detectors were all biased at 150 mV. Similar recovery times are found for this bias condition as in the preceding case. It was possible to observe the decay of the detector voltage of HRC continuously down to about 0.3-mV detector output. This occurred at 2.5 ms as the oscilloscope trace approached the base line. Because of electrical pickup in the range of 50 to 100 μs after the pulse, it was not possible to continuously follow the decay down to this level for the

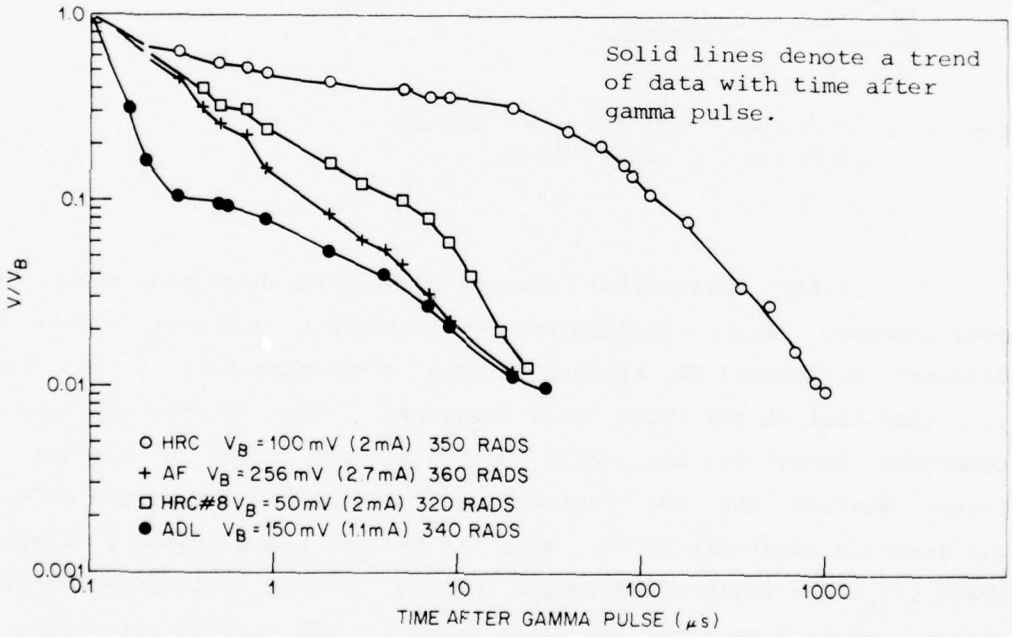

Figure 7. Decay of the detector voltage, scaled by the detector bias voltage, following prompt gamma pulse for the various detectors.

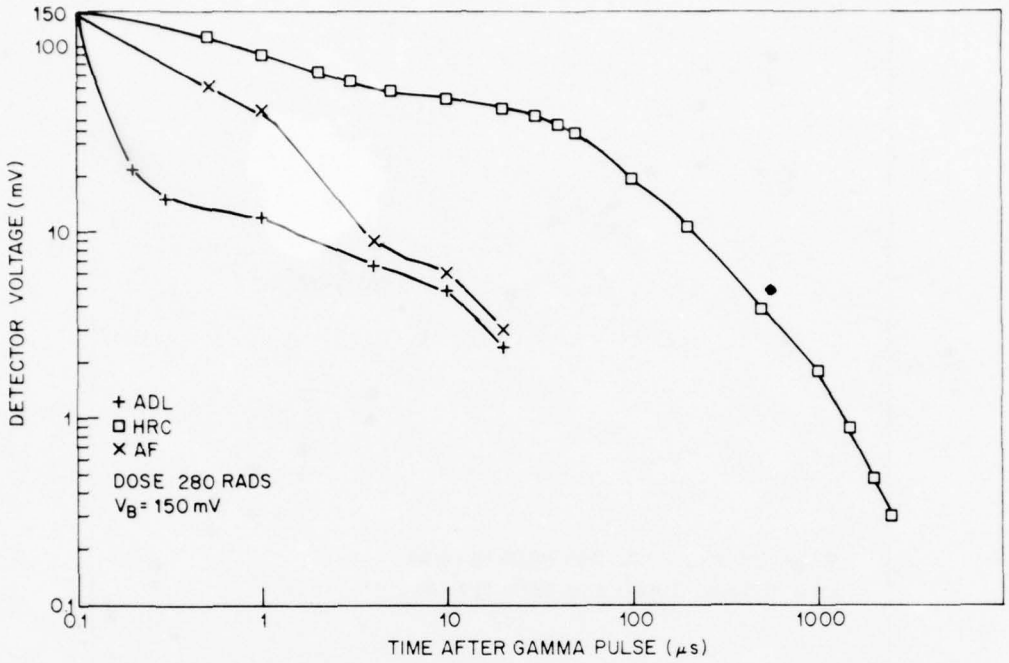

Figure 8. Decay of the detector voltage following the prompt gamma pulse for HRC, AF, and ADL with V_B = 150 mV.

ADL, HRC #8, and AF detectors. For prompt doses greater than 100 rads, a zero bias response of the detector was measurable. When this response is subtracted from the peak response with bias, the peak detector voltage is equal to the bias voltage at the highest doses. The effect of detector bias on the decay curve is shown in figure 9, where the response of the AF detector for two bias conditions is given. It is seen that no significant dependence of the decay rate exists on the bias voltage.

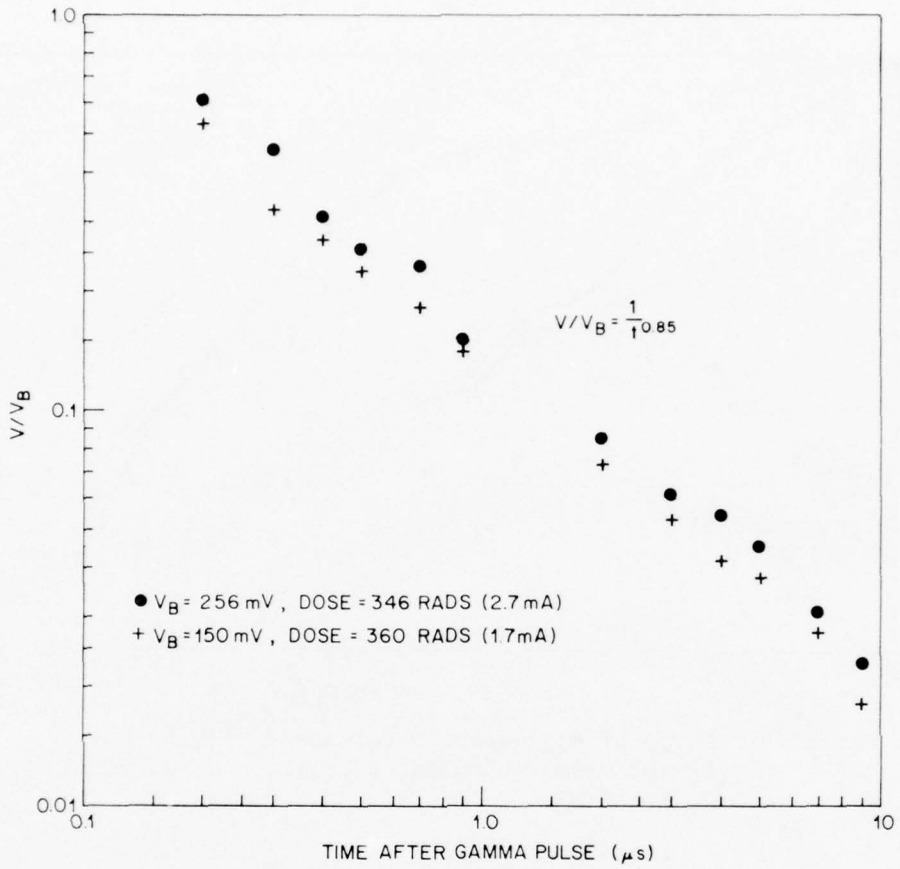

Figure 9. Decay of the detector voltage, scaled by the detector bias, following the prompt gamma pulse for AF with two detector biases, V_B = 256 mV and 150 mV.

The dependence of the detector decay on prompt gamma dose is plotted in figures 10 to 12 for HRC, HRC #8, and AF. Here, V/V_B is plotted on semilog paper, versus time (to ~1 μs) after the pulse. For HRC the decay tail increases monotonically from a dose-independent initial exponential time constant of 200 ns as the dose increases. The initial decay rate of AF and HRC #8, however, appears to be dependent on

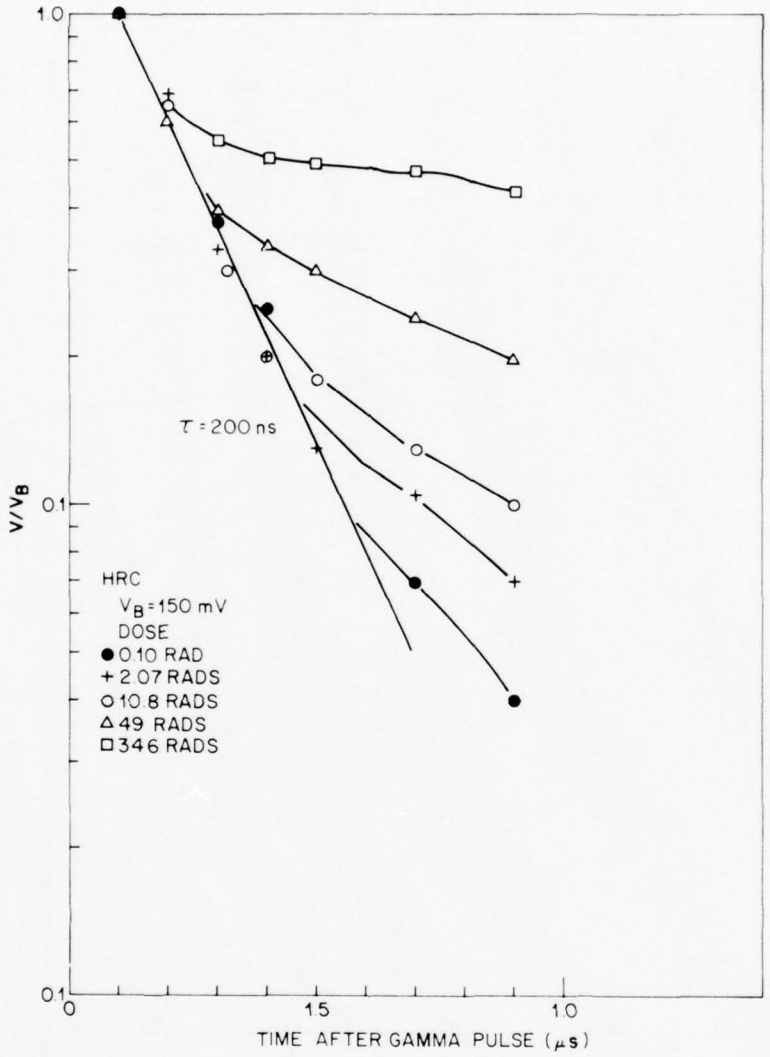

Figure 10. Ratio of detector voltage to detector bias voltage (V/V_B) versus time after the gamma pulse, for HRC with prompt dose as a parameter.

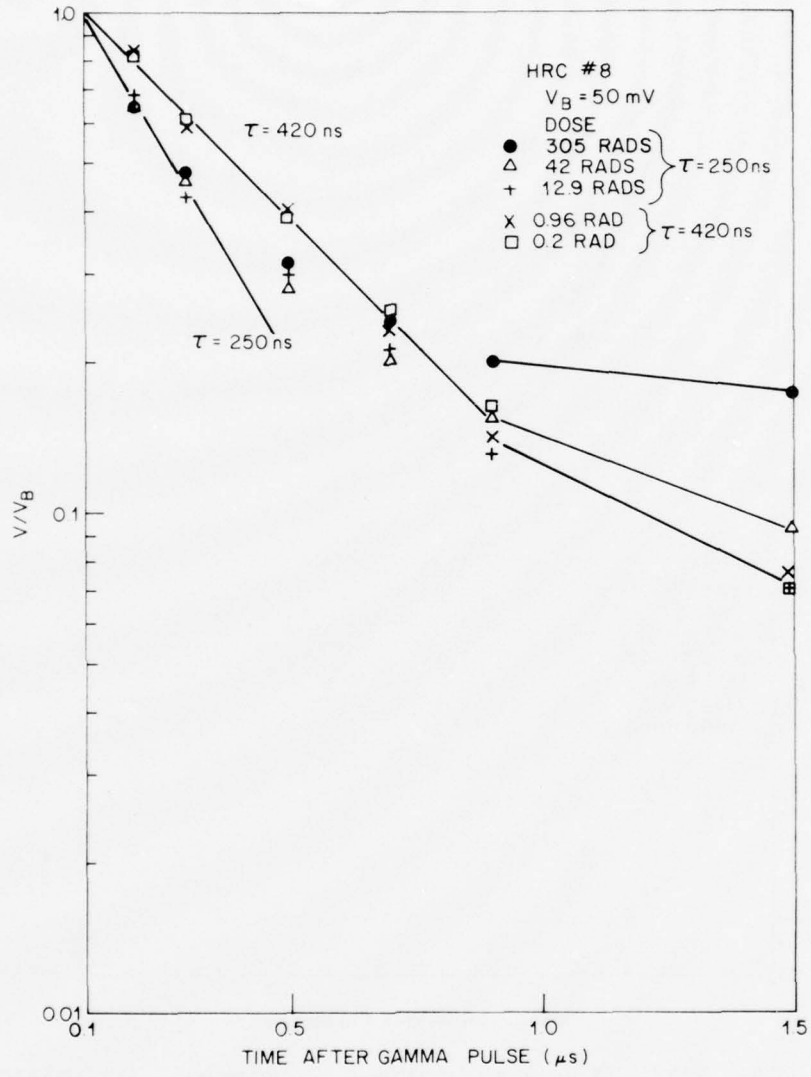

Figure 11. Ratio of detector voltage to detector bias voltage (V/V_B) versus time after the gamma pulse for HRC #8 with prompt dose as a parameter.

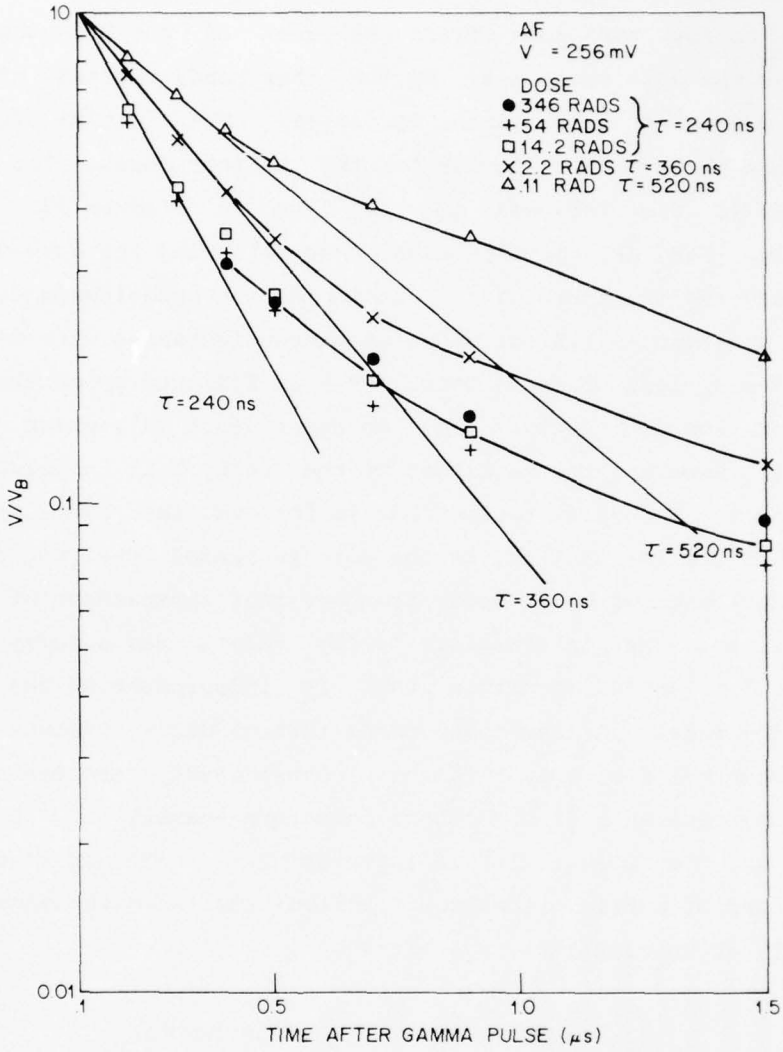

Figure 12. Ratio of detector voltage to detector bias voltage (V/V_B) versus time after the gamma pulse for AF with prompt dose as a parameter.

the dose. As the dose increases, the exponential time constant decreases as seen in figures 11 and 12. The decay tail of HRC #8 appears to follow the same trend as that of the HRC--that is, it increases as the dose increases. On the other hand, the tail of AF (out to 1 μs) decreases as the dose increases. The initial decay-time constants are given in the figures for the various doses. The decay of AF and HRC #8 are followed out to 7 μs in figures 13 and 14, respectively. For AF, it is seen that following the dose dependent initial decay region, there is a region with a dose-independent decay rate (time constant is 1.3 μs) whose magnitude increases with decreasing dose for doses less than 14 rads. This is followed by another region with a yet longer decay time constant (5.5 μs), which is dose independent. However, the magnitude of the decay tail increases as the dose increases. The decay tail of HRC #8 follows the same dependence, as seen in figure 14; that is, as the dose increases the magnitude of the tail increases with the decay-time constant independent of dose and equal to 5.7 μs. The intermediate decay region has a decay constant equal to 0.67 μs and a magnitude that is independent of dose between 12.9 and 305 rads. A dose independent initial decay constant equal to 45 ns was observed for ADL. This is considerably shorter than the initial decay constants of the other detectors--namely 200 to 500 ns, depending on the dose. It is interesting to note that effective optical values of carrier lifetime, τ, calculated[8] from the equation for responsivity at wavelength λ, R_λ, given by,

$$R_\lambda = \eta(\lambda) \cdot \lambda \cdot \tau \cdot V_B/w\ell d \cdot hc \cdot n_o$$

---

[8] *D. Long and J. L. Schmitt, Mercury-Cadmium Telluride and Closely Related Alloys, Semiconductors and Semimetals, Vol. 5, ed. by R. K. Willardson and A. C. Beer, Academic Press, New York (1970), p. 175.*

with the data in table I, yield values comparable with the initial lifetimes obtained in the prompt gamma experiment at the lower dose.

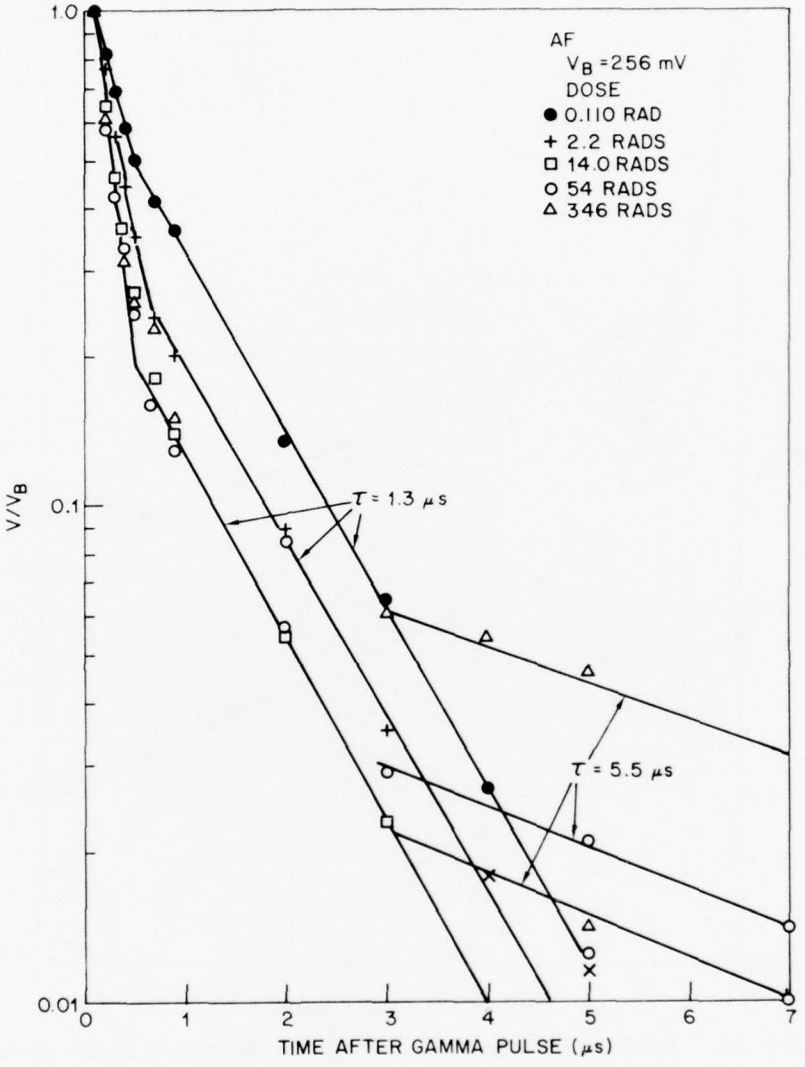

Figure 13. Ratio of detector voltage to detector bias voltage (V/V_B) versus time after the gamma pulse for AF with prompt dose as a parameter.

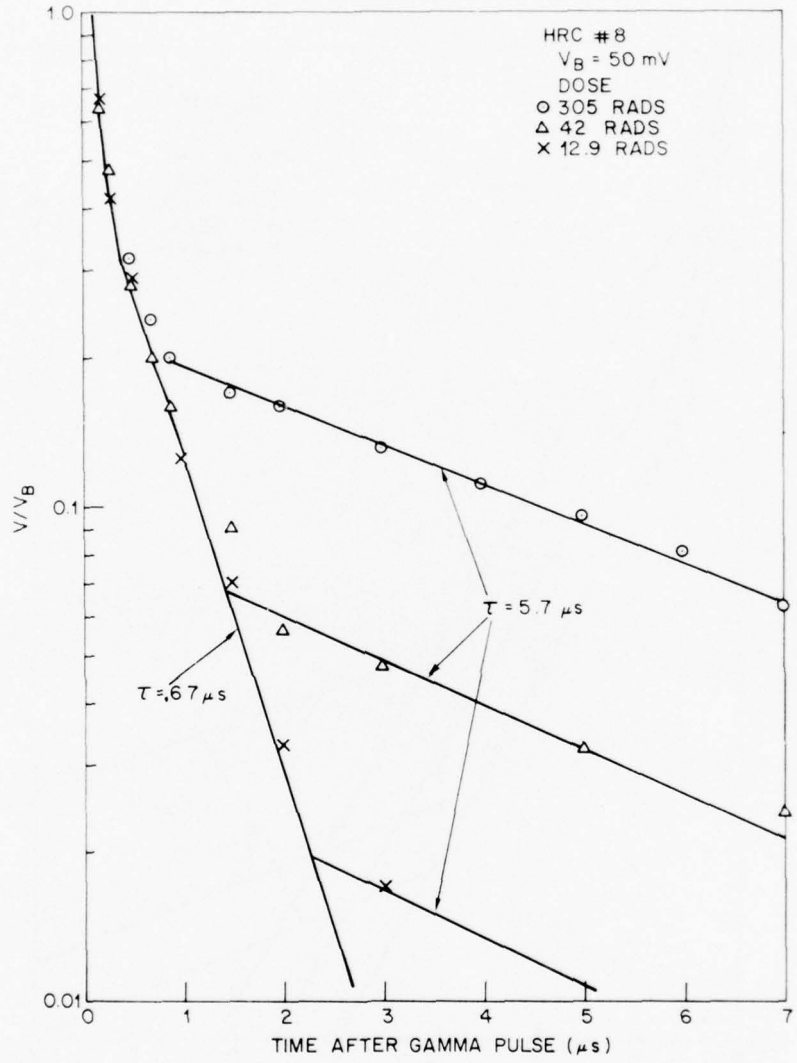

Figure 14. Ratio of detector voltage to detector bias voltage (V/V_B) versus time after gamma pulse for HRC #8 with prompt dose as a parameter.

The effect of prompt gamma dose on the magnitude of peak voltage induced in the detector is given in figures 15 to 18 for the four detectors. The voltage peaks, V_p, which occurred 100 ns after the pulse, were scaled by the bias voltage V_B given in figures 15 to 18. For doses over 100 rads, a zero-bias response was observed, which contributed to the response with bias. When it was subtracted from the biased response, the value of V_p/V_B was unity for all the detectors tested. As seen in figures 15 to 18, all the detectors become saturated for doses in the range of 20 to 40 rads. As the dose decreases below 10 rads the peak voltage decreases. Data taken on the AF detector (fig. 18) show that the peak voltages are not dependent on the detector bias level.

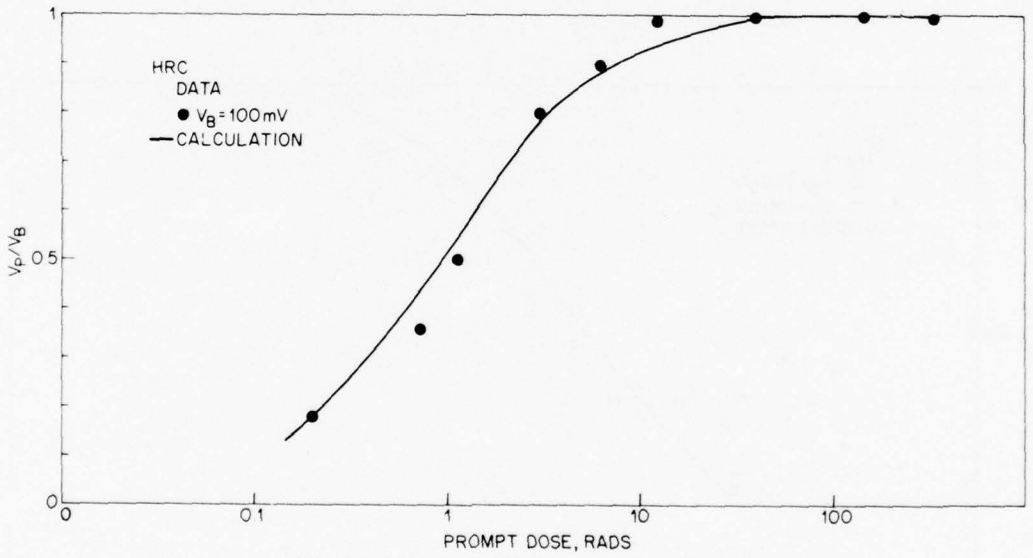

Figure 15. Ratio of peak detector voltage following a prompt gamma pulse to detector bias voltage versus prompt dose for HRC.

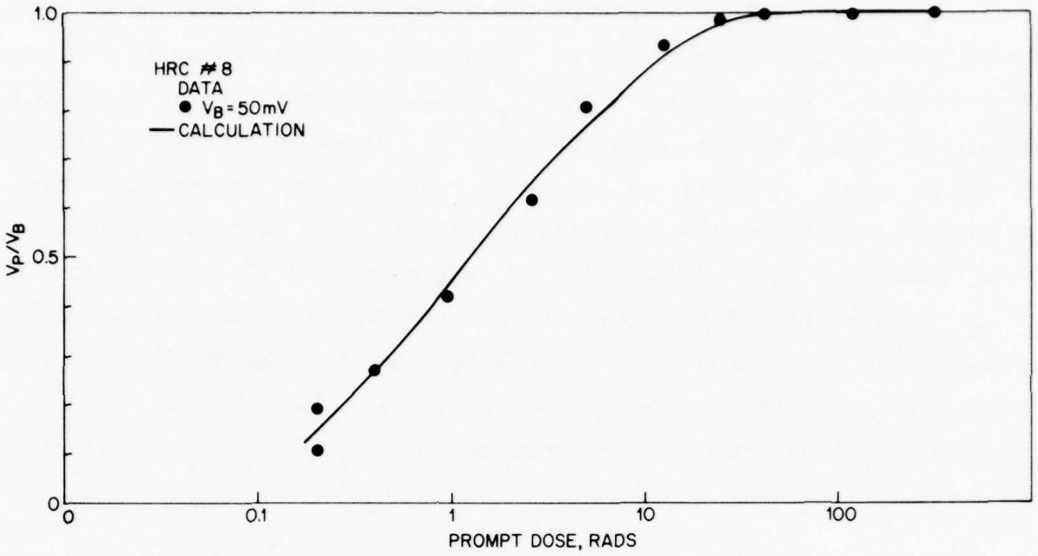

Figure 16. Ratio of peak detector voltage following a prompt gamma pulse to detector bias voltage versus prompt dose for HRC #8.

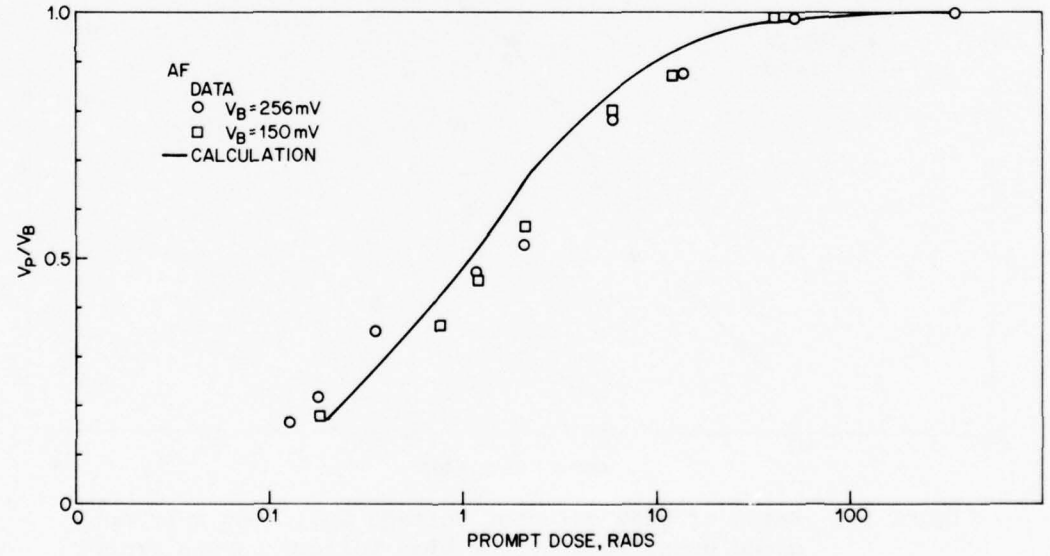

Figure 17. Ratio of peak detector voltage following a prompt gamma pulse to detector bias voltage versus prompt dose for AF.

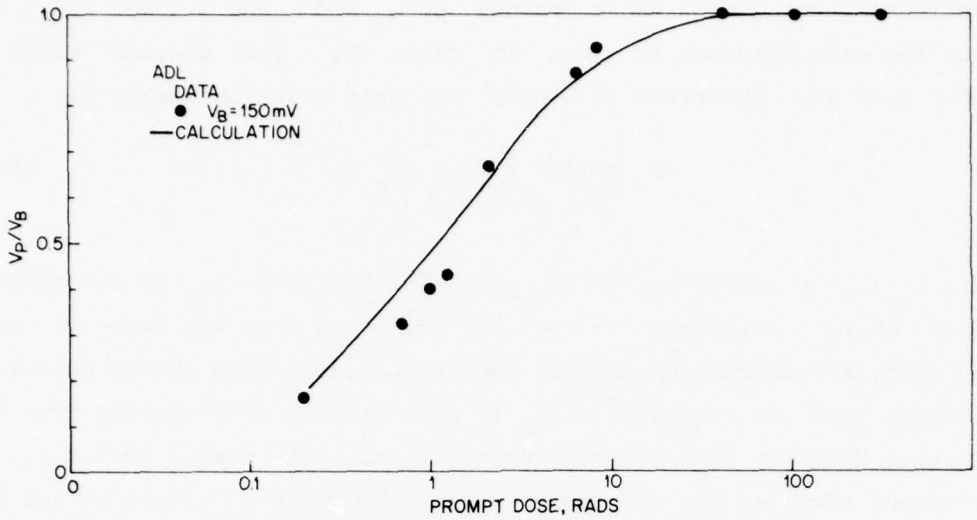

Figure 18. Ratio of peak detector voltage following a prompt gamma pulse to detector bias voltage versus prompt dose for ADL.

6.1.2 Comparison of Theory and Experiments

The dependence of the peak voltage on prompt gamma dose, figures 15 to 18, will be discussed by using equations (7) and (8). Based on these equations, good agreement with data, shown by the solid lines in the figures, can be obtained by using values of n_o, τ, ε_ρ given in table II; n_o was taken from table I. The values of τ were obtained from the initial exponential decay times following prompt gamma doses. The density of $Hg_{0.80}Cd_{0.20}Te$ is 7.5 g/cm^3. The value of t in equation (7) was 100 ns, the time after the pulse at which the peak voltage was measured. The electron-hole pair creation energy ε_ρ was determined as a parameter by requiring that the data satisfy these

equations by using the above values of n_o and τ and t (=100 ns). The value for each detector is given in table II. The average value is 0.36 ± 0.07 eV. According to Klein,[9] the pair creation energy is

$$\varepsilon_\rho = 14/5\ E_g + r\ h\omega_r \quad , \tag{14}$$

where E_g is the energy gap of $Hg_{0.8}Cd_{0.2}Te$, 0.09 eV; $h\omega_r$ is the optical phonon energy calculated to be 0.016 eV,[10] and r is the ratio of mean free paths for intrinsic impact ionization and Raman phonon emission. The first term in equation (14) is made up of a contribution from the intrinsic band gap (E_g) and the residual kinetic energy (9/5 E_g), and the second term is due to phonon losses. By using E_g = 0.09 eV and $h\rho_r$ = 0.016 eV, a value of 0.36 eV is calculated from equation (14) if r = 7. This is similar to the value of r (=8) for Si.[9]

The decay of photoconductivity after cessation of the excitation pulse may proceed by several mechanisms--bimolecular, Shockley-Read, or trap-limited. In the bimolecular process--for example, Auger or radiative recombination--when the radiation-induced excess carrier density is greater than the extrinsic carrier density $\Delta n > n_o$, the decay time constant decreases as the incident

TABLE II. PROMPT GAMMA DATA

Detector	n_o (cm^{-3})	τ (ns)	ε_ρ (eV)
HRC	7×10^{14}	200	0.36
ADL	2.5×10^{14}	45	0.29
AF	8×10^{14}	240	0.43
HRC #8	10^{15}	250	0.37

[9] *C. A. Klein, J. Appl. Phys., 39 (1968), p. 2029.*
[10] *G. Nimtz, G. Bauer, R. Dornhaus, and K. H. Miller, Phys. Rev. B, 10 (1974), p. 3302.*

radiation dose increases.[11] As the decay proceeds, eventually $\Delta n < n_o$ and the decay rate decreases approaching a limiting value.[11] When the decay takes place via defects located in the energy gap, the decay time constant in the high-excitation regime can be independent of excitation intensity depending on the number of defects and on the location of the defects on the energy gap. If the defect density n_t is small ($<n_o$) or if the defect energy coincides with the Fermi level and the number of excess electrons (Δn) equals the number of excess holes (Δp), then the decay proceeds exponentially via Shockley-Read recombination (see Blakemore,[11] page 259). If, however, some of the excited carriers are trapped at defects so that $\Delta n \neq \Delta p$, then the decay may not necessarily be characterized by a single exponential decay constant.[12] A longer decay constant can result, which will depend on the length of time the carriers are trapped at the defect sites and then re-emitted into the conduction band.

The decay curves for the AF and HRC #8 initially follow a bimolecular recombination process, with the decay time constant becoming shorter as the prompt gamma dose increases (see fig. 11 and 12). This occurred for doses >1 rad, which, from equation (6), gives $n > 2 \times 10^{15}$ cm^{-3} and is consistent with $\Delta n > n_o$. The value of the initial decay time constant at the lowest dose is 400 to 500 ns. This is the range for an Auger limited band-to-band recombination process (700 ns).[13] The initial decay constants of the HRC (200 ns) and ADL (45 ns) are independent of dose and are shorter than those of the AF and HRC #8. This may be related to Shockley-Read recombination centers

---

[11] *J. S. Blakemore, Semiconductor Statistics, Pergamon Press, New York (1962), p. 209.*

[12] *R. A. Smith, Semiconductors Cambridge U. Press, Cambridge, MA (1959), p. 308.*

[13] *M. A. Kinch, M. J. Brau, and A. Simmons, J. Appl. Phys., 44 (1973), p. 1649.*

which shunt the bimolecular process. A low carrier concentration such as found for the ADL may be due to compensation and, hence, an inc. ng degree of Shockley-Read process recombination associated with it.[1] As the decay proceeds in the AF and HRC #8, an intermediate region with a dose-independent decay constant is observed for both detectors (fig. 13 and 14) equal to 1.3 and 0.67 μs, respectively. Following this is a region with a decay constant equal to 5.5 μs for both detectors. This longer time constant is probably due to a trapping level. The intermediate region could be due to either the tail of the bimolecular process or the onset of the trapping process.[12] As seen in figures 13 and 14, the decay characteristic follows a series of exponentials with various decay constants. It has been shown that if this is ascribable to a series of trapping processes, then the decay proceeds as $1/t^n$ where n = 1 for a uniform distribution of traps,[14] or n = 2 when the traps are saturated at the beginning of the decay and the cross section of trapping equals the cross section for thermal emission.[15] The data in figures 7 and 9 for AF indicate a $t^{-0.85}$ dependence from 0.1 to 20 μs and are indicative of trapping processes. From figures 9, 13, and 14, the long-time response (>10 μs) of ADL and HRC #8 are similar to that of the AF, indicating that the trapping mechanisms may be similar in these devices. It is noted that each of these detectors was fabricated by a different crystal growing procedure. The short-time response (<1 μs), however, did show differences, especially for ADL as noted above.

---

[12] *R. A. Smith, Semiconductors Cambridge U. Press, Cambridge, MA (1959), p. 308.*

[13] *M. A. Kinch, M. J. Brau, and A. Simmons, J. Appl. Phys., 44 (1973), p. 1649.*

[14] *H. W. Leverenz, An Introduction to Luminescence of Solids, John Wiley and Sons, New York (1950), p. 270.*

[15] *R. H. Bube, Photoconductivity of Solids, John Wiley and Sons, New York (1960), p. 279.*

It is difficult to determine the cause of the long decay time in the HRC detector. Since both the HRC and HRC #8 were fabricated by the same crystal growing procedure, it does not appear to be related to a material characteristic associated with the crystal growth. Long decay times (>milliseconds) are observed in $Hg_{0.8}Cd_{0.2}Te$; but under the experimental conditions of this experiment, two-carrier mode of operation is commonly observed. It is necessary to consider the detector response to luminescence produced by the ionizing radiation incident on detector substrate, windows, and surrounding material (e.g., glass). The HRC was mounted on a ZnS (IRTRAN II) substrate, whereas the AF and HRC #8 detectors were mounted on sapphire. The ZnS, as well as sapphire, is known to be luminescent material when exposed to ionizing radiation.[16,17,18] But at doses considered here (300 rads), it is not expected to produce luminescence large enough to cause a significant detector response.[17] Also, the ADL was mounted on a ZnS substrate and did not display a long decay tail. It is noted that the dewar windows of AF, HRC #8, and ADL (dome) were Ge, which is opaque to visible light, whereas the HRC had an IRTRAN II window, which transmits visible light. At present, however, it is not obvious how this would be responsible for the long decay tail. Finally, the HRC had a ZnS antireflection coating, whereas the surface of HRC #8 and ADL were untreated and the AF was passivated. The condition of the surface is known to be important to the operation of short-wavelength IR HgCdTe detectors in ionizing

---

[16] *D. Curie, Luminescence in Crystals, Methuen, London (1963), p. 298.*

[17] *Radiation Effects in Passive Optical Sensor Components--Final Technical Report--SAMSO TR-74-19 LMSC-B324459 (December 1973); B. Passenheim, Radiance and Attenuation of Luminescence in IR Detector Substrate Material, Army Materials and Mechanics Research Center CTR-74-40 (June 1974).*

[18] *L. P. Randolph, J. N. Lee, and R. B. Oswald, Jr., IEEE Trans. Nucl. Sci., NS-22, No. 6 (1975), p. 2265.*

radiation environments.[19] Possibly the presence of the ZnS coating is responsible for the long decay tail in HRC, either through a direct coupling of the luminescence from the ZnS into the detector or through a surface-induced defect at the detector-coating interface.

6.2 Low-Level Gamma Counting

6.2.1 Data

Oscillograms of individual gamma pulses after being amplified (×200) are shown in figures 19 and 20 for the HRC and ADL detectors, respectively. Note that the decay time of HRC is

Horizontal scale: 100 ns/cm
Vertical scale: 200 mV/cm

Figure 19. Oscillogram of HRC response to single gamma event.

Horizontal scale: 100 ns/cm
Vertical scale: 20 mV/cm

Figure 20. Oscillogram of ADL response to single gamma event.

[19] *Proceedings of Meeting of IRIS Specialty Group on IR Detectors (July 1974): B. H. Breazeale, M. A. Kinch, and M. J. Brau, p. 295; M. M. Blouke and S. R. Borrello, p. 453; A. R. Chandua, B. L. Musicant, R. A. Rotolante, F. Junga, N. Nielsen, J. Pickel, S. Mims, and H. Nobel, p. 479.*

considerably longer than that of the ADL, similar to the prompt gamma response. The peak-pulse height of HRC is larger (by almost a factor of 10) than that for the ADL. Pulse-height distributions of these two detectors in a 2×10^9 $\gamma/cm^2 \cdot s$ (1 rad/s) gamma field are shown in figures 21 and 22. The number of voltage pulses per second with an amplitude greater than some threshold P is plotted on semilog paper versus the threshold level. The dashed lines denote a trend of the data. The HRC detector was oriented with the optical axis parallel to the gamma field; the ADL was perpendicular to the field. Data were also taken on ADL with optical axis oriented 30 deg to the gamma field. Each orientation (of the ADL) gave nearly similar pulse-height distributions. The distributions of both detectors are exponential with the HRC exhibiting a smaller count rate than that of the ADL. Pulse-height distributions could not be measured on HRC #8 and AF.

6.2.2 Discussion and Comparison with Theory

An approximate value of the maximum voltage pulse induced by a single gamma--that is, secondary Compton gamma electron, calculated from equations (9) and (10)--is compared with the measured maximum (see fig. 21 and 22) in table III. The values of ε_ρ were taken from table II and the value of $\Delta E/\Delta x$ = 10 MeV/cm for CdTe[20] was used in equation (10). Agreement within a factor of 3 to 4 is obtained for HRC and ADL, which is satisfactory for this approximate calculation. The values calculated for AF and HRC #8 are too small to be measured with our apparatus, as observed on these detectors.

---

[20] *H. L. Malm, T. W. Raudorf, M. Martini, and K. R. Zamo, IEEE Trans. Nucl. Sci., NS-20, No. 1 (1973), 500.*

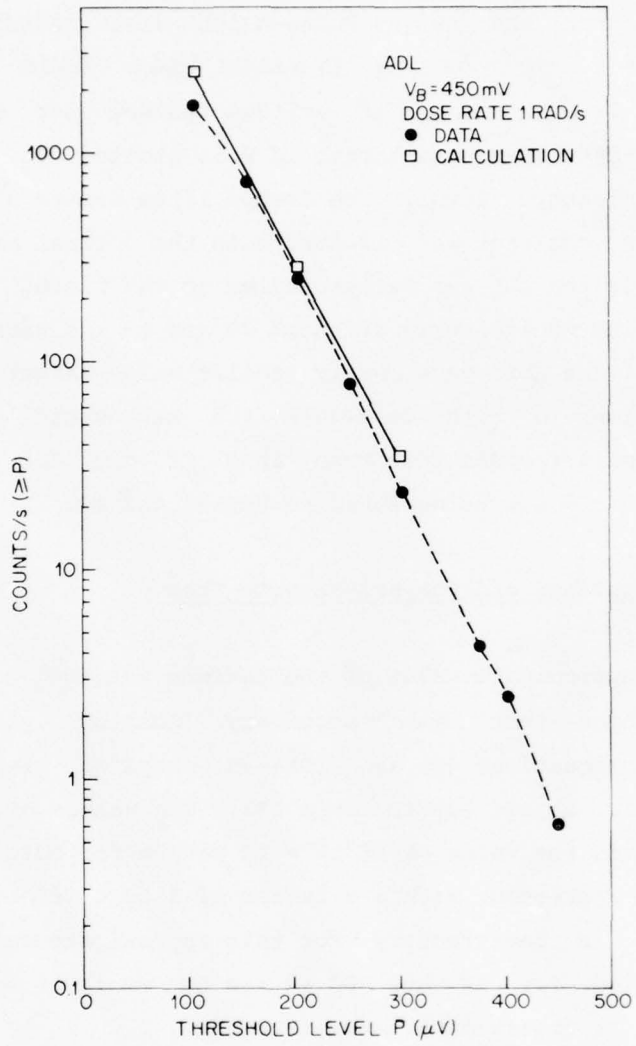

Figure 21. Pulse-height distribution for ADL in 1 rad/s gamma field.

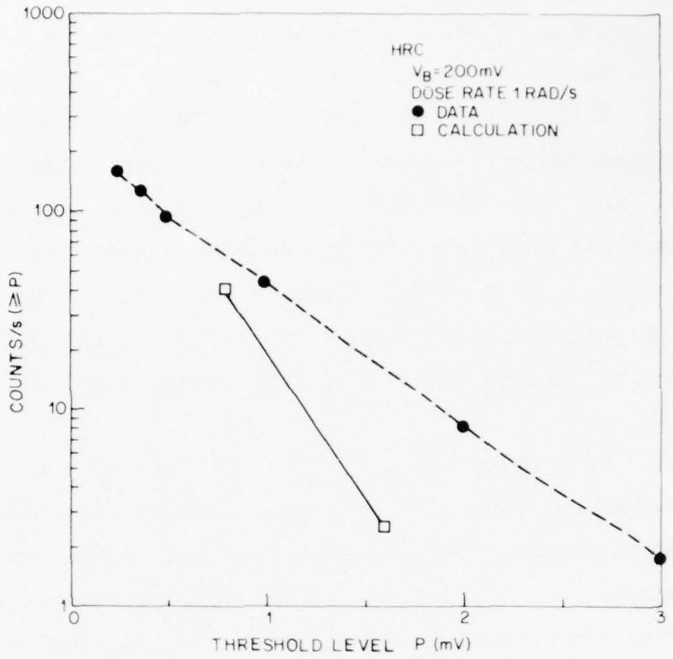

Figure 22. Pulse-height distribution for HRC in 1 rad/s gamma field.

TABLE III. LOW-LEVEL GAMMA-INDUCED PULSE HEIGHT

Detector	wx (cm^2)	n_o (cm^{-3})	V_B (V)	Calculated V_p (μV)	Measured V_p (μV)
HRC	10^{-5}	7×10^{14}	0.195	700	2000
ADL	6.25×10^{-4}	2.5×10^{14}	0.450	100	450
AF	4.5×10^{-3}	8×10^{14}	0.300	1.8	---
HRC #8	6.25×10^{-4}	10^{15}	0.081	3.1	---

The maximum number of counts per second is larger than the value determined from internal events, $\dot{\gamma}\mu\ell\omega d$. For $\dot{\gamma} = 2 \times 10^9\ \gamma/cm^2 \cdot s$ (1 rad/s), $\mu = 0.45\ cm^{-1}$ (taken from Malm et al[20]) (linear absorption coefficient of 1-MeV gamma in $Hg_{0.8}Cd_{0.2}Te$ based on a density of 7.5 g/cm^2) and the detector volumes, the calculated value is 12 counts/s for the HRC and 680 counts/s for the ADL detectors. This is considerably smaller than the largest measured value (see fig. 21 and 22) of 170 counts/s and 1700 counts/s, respectively, for the two detectors and is an indication that a portion of the pulses is due to Compton events originating external to the detector volume.

This is supported by the comparison of the measured pulse-height distribution with the calculated distribution (eq (11)) based on a contribution from external Compton events produced in the surrounding glass. Considering the approximations used in the calculation, good agreement between theory (solid line) and experiment (dashed line) is seen. These results were obtained by using the values of ε_ρ and n_o found in table II. Due to the isotropic penetrating nature of the radiation, the calculation also predicts no orientation dependence of the distribution, as observed. The agreement between the measured and calculated distribution is found to be better for the ADL detector than that found for the HRC detector. It is noted that the surface of the ADL was untreated, whereas the surface of the HRC had a ZnS coating. No account of surface treatment was taken in the calculation.

---

[20] *H. L. Malm, T. W. Raudorf, M. Martini, and K. R. Zamo, IEEE Trans. Nucl. Sci., NS-20 (1973), 500.*

6.3 High-Level Gamma Noise

6.3.1 Data

The rms gamma-induced noise voltage induced in the detector is plotted against dose rate (rads/s) for the four detectors in figures 23 to 26. The bandwidth of the voltage measurement is 4 MHz. The gamma-induced rms noise voltage V_γ was obtained from V_m, the rms voltmeter reading with the detector in the gamma field, and V_o, the reading with the detector out of the gamma field according to the following equation:

$$V_\gamma = \sqrt{V_m^2 - V_o^2} \tag{15}$$

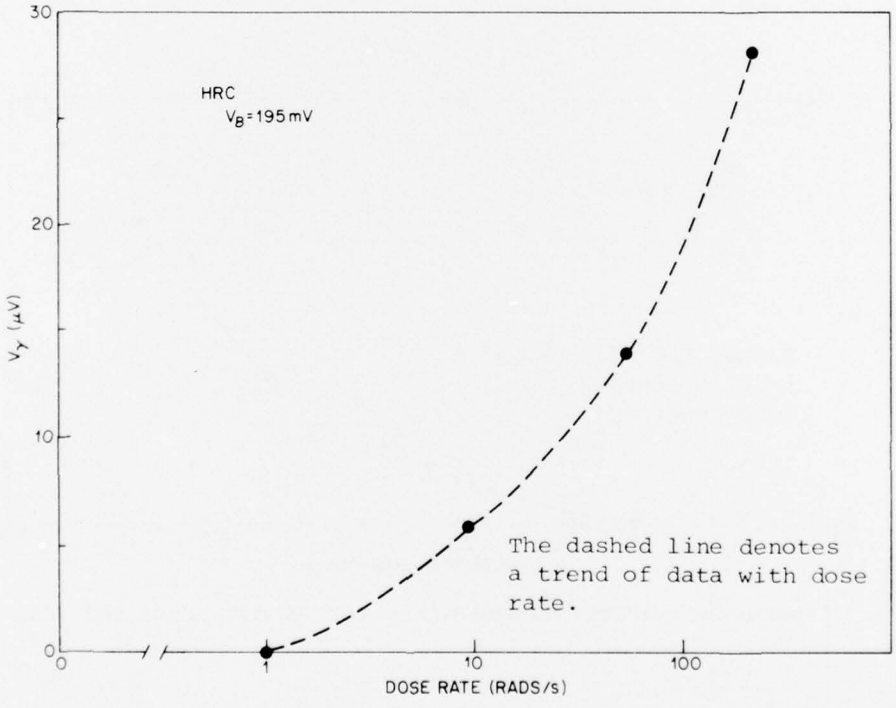

Figure 23. Gamma-induced noise versus dose rate for HRC.

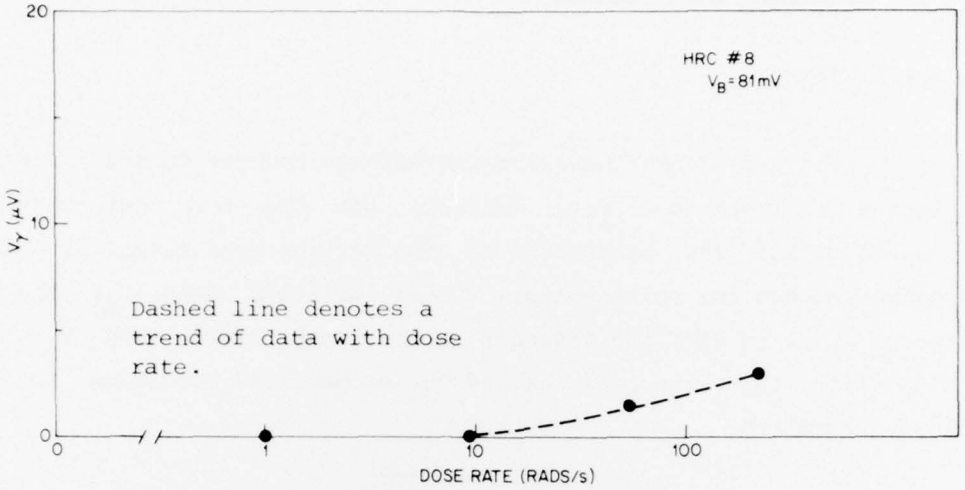

Figure 24. Gamma-induced noise versus dose rate for HRC #8.

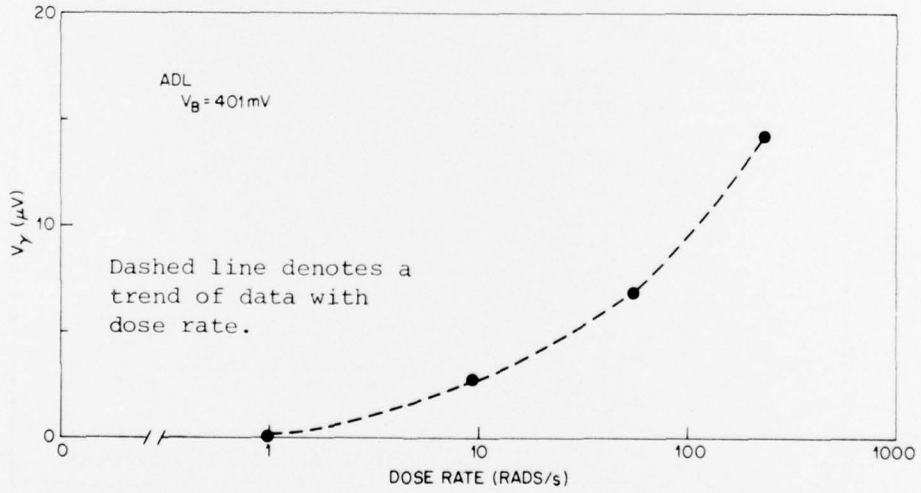

Figure 25. Gamma-induced noise versus dose rate for ADL.

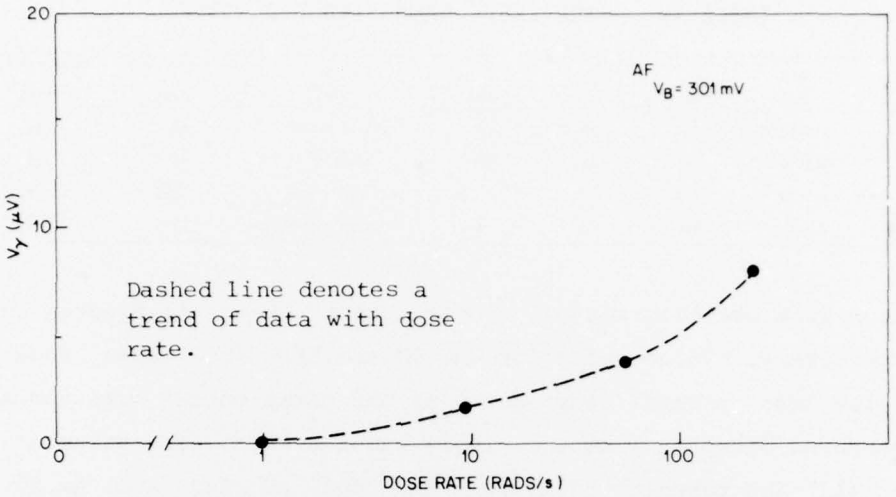

Figure 26. Gamma-induced noise versus dose rate for AF.

The value of V_o was easily obtained by lowering the ^{60}Co source into the pool after V_m was measured. The highest dose rate at which the measurement was performed was 220 rads/s. The largest noise voltage was induced in HRC, whereas the smallest was induced on HRC #8. Since many detector applications require operation at reduced bandwidth, the measurement was performed with a 420-Hz filter in the circuit. This had the effect of reducing the radiation-induced noise below the sensitivity of the measurement for all detectors except for the HRC, which gave a value of 1 μV.

6.3.2 Comparison of Theory and Experiments

The experimental values of the rms gamma-induced noise measured at 220 rads/s are compared in table IV with the theoretical values, based on equation (12). The values of V_p were taken from the calculated values in table III (eq (9) and (10)), by using ε_p from the prompt gamma experiments (table II). The values of τ for HRC and ADL

TABLE IV. HIGH-LEVEL GAMMA-INDUCED NOISE

Detector	wtd (cm^3)	τ (ns)	K	V_p (μV)	B (Hz)	Calculated V_γ (μV)	Measured V_γ (μV)
HRC	1.2×10^{-8}	150	20	700	$1/2\pi\tau=1.06\times10^6$	65	28
ADL	7.5×10^{-7}	20	10	90	$\Delta f=4\times10^6$	15	14
AF	1.1×10^{-5}	520	10	1.8	$1/2\pi\tau=0.3\times10^6$	6.8	8.0
HRC #8	7.5×10^{-7}	420	10	3.1	$1/2\pi\tau=0.37\times10^6$	2.8	2.9

were taken from oscillograms of single gamma events in figures 19 and 20, respectively. Values of τ for HRC #8 and AF were taken from the initial low dose prompt gamma data, as the gamma pulses were too small to be measured directly from the single gamma events. The value of K in equation (13) was taken to be 20 for HRC and 10 for ADL, based on a comparison of the extrapolation of the count rate to zero pulse height in the experimental pulse height distribution (fig. 21 and 22) with the calculated internal event rate; K was taken to be 10 for AF and HRC #8. Considering the number of parameters in the calculation, there is very good agreement between theory and experiment for all the detectors even with the factor-of-two difference for HRC. Reducing the bandwidth to 420 Hz predicts a value of V_γ equal to 1.3 μV for the HRC at 220 rads/s. The measured value was 1 μV.

7. CONCLUSIONS

The results of these experiments--prompt gamma, low-level counting and high-level gamma-induced noise--indicate that the average value of the electron-hole pair creation energy ε_ρ of 0.09 eV $Hg_{0.8}Cd_{0.2}Te$ is 0.36 $\pm$ 0.07 eV. This is consistent with the value predicted by Klein.[9] Analysis of gamma-counting and noise experiments indicates that

[9] *C. A. Klein, J. Appl. Phys., 39 (1968), p. 2029.*

the majority of the gamma events originates from Compton interactions in the surrounding material--for example glass dewar external to the detector. Initial decay characteristics of the detector response following a prompt gamma pulse appear to depend on the detector material, proceeding either through a bimolecular or a Shockley-Read recombination process. At longer times, trap-limited processes become operative in which the fractional level of decay reaches the same value of all the material-preparation techniques evaluated. This applies to detectors in which the surface was left untreated or was passivated. A detector with the surface treated with a ZnS antireflection coating, however, exhibited an enhanced long time decay response at the largest gamma doses.

ACKNOWLEDGEMENT

The author thanks F. Nelson of HDL for his technical assistance during these experiments, G. Poncelet of Aeronutronic Ford, Inc., for use of the 10-MHz preamplifier, and Aeronutronic Ford, Inc., Honeywell Research Corporate Radiation Center, and A. D. Little, Inc., for use of HgCdTe detectors.

LITERATURE CITED

(1) C. Harman, J. Electronic Mat., 1, (1972). p. 230.

(2) J. Steininger, Proceedings of Meeting of IRIS Specialty Group on IR Detectors (13-15 March 1973) p. 33.

(3) P. W. Kruse, Appl. Optics, 4 (1965), p. 687.

(4) R. A. Rotolante, R. P. Muroska, and G. E. Keiser, Radiation Effects in Intrinsic Photodetector Systems (U), Honeywell Radiation Center AMMRC CTR 73-46 (December 1973). (SECRET)

(5) J. W. Haffner, Presented at 1975 IEEE, Annual Conference Nuclear and Space Radiation Effects, Poster Session Paper (14-17 July 1975).

(6) Detector Test Program Final Report, Vol. 1, LMSC-B303910 Contract FO4701-70-C-0227 (August 1972).

(7) J. C. Pickel and M. D. Petroff, IEEE Trans. Nucl. Sci., NS-22, No. 6 (1975), p. 2456.

(8) D. Long and J. L. Schmitt, Mercury-Cadmium Telluride and Closely Related Alloys, Semiconductors and Semimetals, Vol. 5, ed. by R. K. Willardson and A. C. Beer, Academic Press, New York (1970), p. 175.

(9) C. A. Klein, J. Appl. Phys., 39 (1968), p. 2029.

(10) G. Nimtz, G. Bauer, R. Dornhaus, and K. H. Miller, Phys. Rev. B, 10 (1974), p. 3302.

(11) J. S. Blakemore, Semiconductor Statistics, Pergamon Press, New York (1962), p. 209.

(12) R. A. Smith, Semiconductors, Cambridge U. Press, Cambridge, MA (1959), p. 308.

(13) M. A. Kinch, M. J. Brau, and A. Simmons, J. Appl. Phys., 44 (1973), p. 1649.

(14) H. W. Leverenz, An Introduction to Luminescence of Solids, John Wiley and Sons, New York (1950), p. 270.

(15) R. H. Bube, Photoconductivity of Solids, John Wiley and Sons, New York (1960), p. 279.

(16) D. Curie, Luminescence in Crystals, Methuen, London (1963), p. 298.

(17) Radiation Effects in Passive Optical Sensor Components--Final Technical Report--SAMSO TR-74-19 LMSC-B324459 (December 1973); B. Passenheim, Radiance and Attenuation of Luminescence in IR Detector Substrate Material, Army Materials and Mechanics Research Center CTR-74-40 (June 1974).

(18) L. P. Randolph, J. N. Lee, and R. B. Oswald, Jr., IEEE Trans. Nucl. Sci., NS-22, No. 6 (1975), p. 2265.

(19) Proceedings of Meeting of IRIS Specialty Group on IR Detectors (July 1974): B. H. Breazeale, M. A. Kinch, and M. J. Brau, p. 295; M. M. Blouke and S. R. Borrello, p. 453; A. R. Chandua, B. L. Musicant, R. A. Rotolante, F. Junga, N. Nielsen, J. Pickel, S. Mims, and H. Nobel, p. 479.

(20) H. L. Malm, T. W. Raudorf, M. Martini, and K. R. Zamo, IEEE Trans. Nucl. Sci., NS-20 No. 1 (1973), p. 500.

DISTRIBUTION

DEFENSE DOCUMENTATION CENTER
CAMERON STATION, BUILDING 5
ALEXANDRIA, VA 22314
ATTN DDC-TCA (12 COPIES)

COMMANDER
USA RSCH & STD GP (EUR)
BOX 65
FPO NEW YORK 09510
ATTN LTC JAMES M. KENNEDY, JR.
CHIEF, PHYSICS & MATH BRANCH

COMMANDER
US ARMY MATERIEL DEVELOPMENT
& READINESS COMMAND
5001 EISENHOWER AVENUE
ALEXANDRIA, VA 22333
ATTN DRXAM-TL, HQ TECH LIBRARY
ATTN DRCRD-TT, R. ZENTNER

COMMANDER
USA ARMAMENT COMMAND
ROCK ISLAND, IL 61201
ATTN DRSAR-ASF, FUZE DIV
ATTN DRSAR-RDF, SYS DEV DIV - FUZES

COMMANDER
USA MISSILE & MUNITIONS CENTER & SCHOOL
REDSTONE ARSENAL, AL 35809
ATTN ATSK-CTD-F

DIRECTOR
DEFENSE NUCLEAR AGENCY
WASHINGTON, DC 20305
ATTN SPAS, CAPT R. DAVIS

COMMANDER
FIELD COMMAND
DEFENSE NUCLEAR AGENCY
KIRTLAND AFB, NM 87115
ATTN FCPR

DIRECTOR
DEFENSE INTELLIGENCE AGENCY
WASHINGTON, DC 20301
ATTN DS-4A2

CHIEF
LIVERMORE DIVISION,
FIELD COMMAND DNA
LAWRENCE LIVERMORE LABORATORY
P.O. BOX 808
LIVERMORE, CA 94550
ATTN DOCUMENT CONTROL FOR L-395

DIRECTOR
NATIONAL SECURITY AGENCY
FT. GEORGE G. MEADE, MD 20755
ATTN TDL
ATTN O. O. VAN GUNTEN, R-425

WEAPONS SYSTEMS EVALUATION GROUP
400 ARMY NAVY DIRVE
ARLINGTON, VA 22202
ATTN DOCUMENT CONTROL

OFFICE, CHIEF OF RESEARCH, DEVELOPMENT
AND ACQUISITION
DEPARTMENT OF THE ARMY
WASHINGTON, DC 20310
ATTN DAMA-CSS-D, DR. J. BRYANT

DIRECTOR OF DEFENSE RESEARCH
AND ENGINEERING
WASHINGTON, DC 20301
ATTN MR. J. PERSH, DEPUTY FOR MATERIALS
& STRUCTURES (ENGR TECHNOLOGY)

DIRECTOR
DEFENSE ADVANCED RESEARCH PROJECTS AGENCY
1400 WILSON BOULEVARD
ARLINGTON, VA 22209
ATTN CAPT J. JUSTICS

DIRECTOR
US ARMY BALLISTIC RESEARCH LABORATORIES
ABERDEEN PROVING GROUND, MD 21005
ATTN DRXRD-BVL, DAVID L. RIGOTTI
ATTN TECH LIB, EDWARD BAICY
ATTN DRXBR-AM, W. R. VAN ANTWERP
ATTN DRXBR-VL, JOHN W. KINCH
ATTN DRXBR-VL, ROBERT L. HARRISON
ATTN DRXBR-X, JULIUS J. MESZAROS

DIRECTOR
BALLISTIC MISSILE DEFENSE ADVANCED
TECHNOLOGY CENTER
P.O. BOX 1500
HUNTSVILLE, AL 35807
ATTN ATC-S, M. CAPPS
ATTN ATC-O, F. HOKE
ATTN B. KELLEY
ATTN W. GIBSON (5 COPIES)

BALLISTIC MISSILE DEFENSE PROGRAM OFFICE
COMMONWEALTH BUILDING
1300 WILSON BOULEVARD
ARLINGTON, VA 22209
ATTN DACS-BMT

COMMANDER
BALLISTIC MISSILE DEFENSE SYSTEMS COMMAND
P.O. BOX 1500
HUNTSVILLE, AL 35807
ATTN BMDSC-TEN, NOAH HURST

COMMANDER
US ARMY COMBAT DEVELOPMENT COMMAND
INSTITUTE OF NUCLEAR STUDIES
FORT BLISS, TX 79916
ATTN TECHNICAL LIBRARY

DIRECTOR
ARMY MATERIALS AND MECHANICS RESEARCH CENTER
WATERTOWN, MA 02172
ATTN DRXMR-H, J. A. HOFMANN
ATTN DRXMR-PL
ATTN DRXMR-AP
ATTN DRXMR-PR
ATTN DRXMR-CT

COMMANDER
PICATINNY ARSENAL
DOVER, NJ 07801
ATTN SARPA-ND-N
ATTN SARPA-ND-W
ATTN SARPA-TN, BURTON V. FRANKS
ATTN SARPA-FR-E, LOUIS AVRAMI

COMMANDER
US ARMY ELECTRONICS COMMAND
FORT MONMOUTH, NJ 07703
ATTN DRSEL-TL-EN, ROBERT LUX

DIRECTOR
NAVAL ELECTRONICS LABORATORY CENTER
271 CATALINA BOULEVARD
SAN DIEGO, CA 92152
ATTN CODE 4600, W. L. EISENMAN

COMMANDER
US ARMY MISSILE COMMAND
REDSTONE ARSENAL
HUNTSVILLE, AL 35809
ATTN DRSMI-RGP, HUGH GREEN
ATTN DRCPM-LCEX,
HOWARD H. HENRIKSEN
ATTN DRSMI-RRR, FAISON P. GIBSON

COMMANDER
US ARMY MOBILITY EQUIPMENT
R & D CENTER
FORT BELVOIR, VA 22060
ATTN STSFB-MW, JOHN W. BUND, JR.

CHIEF
US ARMY NUCLEAR AND CHEMICAL
SURETY GROUP
BLDG 2073, NORTH AREA
FORT BELVOIR, VA 22060
ATTN MOSG-ND, MAJ S. W. WINSLOW

COMMANDER
US ARMY NUCLEAR AGENCY
FORT BLISS, TX 79916
ATTN ATCN-W, LTC L. A. SLUGA

PROJECT MANAGER
US ARMY TACTICAL DATA SYSTEMS, DARCOM
FT. MONMOUTH, NJ 07703
ATTN DRCPN-TDS-SD, DWAINE B. HUEWE

SAMSO/DY
POST OFFICE BOX 92960
WORLDWAY POSTAL CENTER
LOS ANGELES, CA 90009
ATTN DYS, MAJ LARRY A. DARDA
ATTN DYS, CAPT W. SCHOBER

SAMSO/SZSS
LOS ANGELES AIR FORCE STATION, CA 90009
ATTN MAJOR PETER SIVGALS

ADVISORY GROUP ON ELECTRON DIVICES
201 VARICK STREET
NEW YORK, NY 10014

CHIEF OF NAVAL RESEARCH
DEPARTMENT OF THE NAVY
ARLINGTON, VA 22217
ATTN CODE 421, D. W. PADGETT
ATTN CODE 427

DIRECTOR
NAVAL RESEARCH LABORATORY
WASHINGTON, DC 20375
ATTN CODE 6631, JAMES C. RITTER
ATTN CODE 4004, EMANUAL L. BRANCATO
ATTN CODE 7701, JACK D. BROWN
ATTN CODE 6210, J. DAVEY
ATTN CODE 5216, E. WOLIKI
ATTN N. WILSEY
ATTN CODE 5260, D. BARBE

COMMANDER
NAVAL ELECTRONIC SYSTEMS COMMAND
HEADQUARTERS
WASHINGTON, DC 20360
ATTN CODE 504510
ATTN ELEX 05323, C. F. WATKINS
ATTN PME 117-21

COMMANDING OFFICER
NAVAL INTELLIGENCE SUPPORT CENTER
4301 SUITLAND ROAD, BLDG 5
WASHINGTON, DC 20390
ATTN P. ALEXANDER

COMMANDER
NAVAL SEA SYSTEMS COMMAND
NAVY DEPARTMENT
WASHINGTON, DC 20362
ATTN SEA-9931, R. LANE
ATTN SEA-03331, M. KINNA

COMMANDER
NAVAL SHIP ENGINEERING CENTER
CENTER BUILDING
HYATTSVILLE, MD 20782
ATTN CODE 617402, E. DUFFY

COMMANDER
NAVAL SURFACE WEAPONS CENTER
DAHLGREN LABORATORY
DAHLGREN, VA 22448
ATTN W. H. HOLT

COMMANDER
NAVAL SURFACE WEAPONS CENTER
WHITE OAK LABORATORY
SILVER SPRING, MD 20910
ATTN F. E. WARNOCK
ATTN R. A. SMITH
ATTN M. C. PETREE
ATTN J. LOWNEY

COMMANDER
AIR FORCE AVIONICS LABORATORY
WRIGHT-PATTERSON AIR FORCE BASE, OH 45433
ATTN AFAL/TEO, R. PICKENPAUGH
ATTN AFAL-TEA, HANS J. HENNECKE

AF MATERIALS LAB, AFSC
WRIGHT-PATTERSON AFB, OH 45433
ATTN LTE
ATTN AFML/LPO, R. HICKMOTT

AF WEAPONS LABORATORY, AFSC
KIRTLAND AFB, NM 87117
ATTN SAB
ATTN J. S. NICHOLS
ATTN WLRP, LTC D. YOUNG

AF CAMBRIDGE RSCH LABS, AFSC
L. G. HANSCOM FIELD
BEDFORD, MA 01730
ATTN EMERY CORMIER
ATTN B. BUCHANAN
ATTN D. NEAMAN
ATTN F. SHEPARD

SAMSO/YD
POST OFFICE BOX 92960
WORLDWAY POSTAL CENTER
LOS ANGELES, CA 90009
ATTN YDD, MAJ M. F. SCHNEIDER

COMMANDER IN CHIEF
STRATEGIC AIR COMMAND
OFFUTT AFB, NB 68113
ATTN XPFS, MAJ B. G. STEPHAN

LOS ALAMOS SCIENTIFIC LAB
P.O. BOX 1663
LOS ALAMOS, NM 87545
ATTN DOC CON FOR TRUCE NOEL
ATTN DOC CON FOR J. A. FREED
ATTN DOC CON FOR M. M. HOFFMAN

SANDIA LABORATORIES
LIVERMORE LABORATORY
P.O. BOX 808
LIVERMORE, CA 94550
ATTN DOC CON FOR T. A. DELLIN

SANDIA LABORATORIES
P.O. BOX 5800
ALBUQUERQUE, NM 87115
ATTN DOC CON FOR C. J. MACCALLUM
ATTN DOC CON FOR
J. V. WALER, 5220
ATTN DOC CON FOR ORG 1933,
F. COPPAGE
ATTN H. SANDER

CENTRAL INTELLIGENCE AGENCY
ATTN: RD/SI RM 5G48, HQ BLDG
WASHINGTON, DC 20505
ATTN ALICE A. PADGETT

AEROJET ELECTRO-SYSTEMS CO. DIV
AEROJET-GENERAL CORPORATION
P.O. BOX 296
AZUSA, CA 91702
ATTN THOMAS D. HANSCOME,
B170/D6711
ATTN C. PARRY, BLDG 53, DEPT 6201

AERONUTRONIC FORD CORPORATION
AERONUTRONICS DIVISION
FORD ROAD
NEWPORT BEACH, CA 92663
ATTN J. ROSCHEN
ATTN G. PONCELET
ATTN L. JOHNSON
ATTN F. FISHER

AEROSPACE CORPORATION
P.O. BOX 92957
LOS ANGELES, CA 90009
ATTN I. M. GARFUNKEL
ATTN W. W. WILLIS
ATTN M. J. BERNSTEIN
ATTN LIBRARY
ATTN J. REINHEIMER
ATTN L. W. AUKERMAN
ATTN P. SCHALL

THE BDM CORPORATION
P.O. BOX 9274
ALBUQUERQUE INTERNATIONAL
ALBUQUERQUE, NM 87119
ATTN T. H. NEIGHBORS

THE BOEING COMPANY
P.O. BOX 3707
SEATTLE, WA 98124
ATTN D. L. DYE, MS 37-75
ATTN H. W. WICKLEIN, 17-11
ATTN AEROSPACE LIBRARY
ATTN R. S. CALDWELL, 2R-00

THE BOEING COMPANY
AEROSPACE GROUP
P.O. BOX 3999
SEATTLE, WA 98124
ATTN K. NORSWORTHY, MS 8H12

GEANAKOS LTD.
P.O. BOX 6346
ORANGE, CA 92667
ATTN J. GEANAKOS

GENERAL ELECTRIC CORPORATION
SPACE DIVISION
VALLEY FORGE SPACE CENTER
GODDARD BLVD, KING OF PRUSSIA
P.O. BOX 8555
PHILADELPHIA, PA 19101
ATTN J. L. ANDREWS

GENERAL ELECTRIC COMPANY
RE-ENTRY/ENVIRONMENTAL SYS DIV
P.O. BOX 7722
PHILADELPHIA, PA 19101
ATTN R. V. BENEDICT

GENERAL ELECTRIC COMPANY
TEMPO-CTR. FOR ADVANCED STUDIES
816 STATE STREET (PO DRAWER QQ)
SANTA BARBARA, CA 93102
ATTN DASIAC
ATTN M. ESPIG
ATTN R. R. RUTHERFORD
ATTN MACK STANTON

GENERAL ELECTRIC CO.-TEMPO
ATTN DASIAC
C/O DEFENSE NUCLEAR AGENCY
6801 TELEGRAPH ROAD
ALEXANDRIA, VA 22310
ATTN W. ALFONTE

HONEYWELL INC.
RADIATION CENTER
2 FORBES ROAD
LEXINGTON, MA 02173
ATTN J. SCHLICKMAN
ATTN M. REINE
ATTN T. T. S. WONG

HONEYWELL INC.
SYSTEMS AND RESEARCH DIVISION
2700 RIDGEWAY PARKWAY
MINNEAPOLIS, MN 55413
ATTN ROGER HEINISCH

HUGHES AIRCRAFT COMPANY
AEROSPACE GROUP
CULVER CITY, CA 90230
ATTN G. AROYAN, BLDG 5, MS B118
ATTN G. AUTIO, BLDG 5, MS B146

HUGHES AIRCRAFT COMPANY
SPACE SYSTEMS DIVISION
P.O. BOX 92919
LOS ANGELES, CA 90009
ATTN E. C. SMITH, MS A620
ATTN W. W. SCOTT, A1080

HUGHES AIRCRAFT COMPANY
500 SUPERIOR AVENUE
NEWPORT BEACH, CA 92663
ATTN K. G. AUBUCHON
ATTN E. HARARI

INSTITUTE OF DEFENSE ANALYSIS
400 ARMY-NAVY DRIVE
ARLINGTON, VA 22202
ATTN A. D. SCHNITZLER

IBM CORPORATION
ROUTE 17C
OWEGO, NY 13827
ATTN FRANK FRANKOVSKY

INTELCOM RAD, TECH
P.O. BOX 80187
SAN DIEGO, CA 92138
ATTN J. A. NABER
ATTN R. H. STAHL
ATTN R. L. MERTZ
ATTN T. M. FLANAGAN
ATTN A. KALMA

ION PHYSICS CORPORATION
SOUTH BEDFORD STREET
BURLINGTON, MA 01803
ATTN ROBERT D. EVANS

KAMAN SCIENCES CORPORATION
P.O. BOX 7463
COLORADO SPRINGS, CO 80933
ATTN A. P. BRIDGES
ATTN W. E. WARE
ATTN D. H. BRYCE
ATTN P. L. JESSEN

ARTHUR D. LITTLE, INC.
ACORN PARK
CAMBRIDGE, MA 02140
ATTN DETECTION SCIENCES GROUP, J. SLAWEK
ATTN D. STANFILL

LOCKHEED MISSILES AND SPACE COMPANY
3251 HANOVER STREET
PALO ALTO, CA 94304
ATTN K. CUFF

LOCKHEED MISSILES/SPACE CO.
P.O. BOX 504
SUNNYVALE, CA 94088
ATTN E. A. SMITH, DEPT 85-85
ATTN P. H. HART, 81-14
ATTN G. F. HEATH, D/81-14
ATTN B. T. KIMURA, 81-14
ATTN H. L. SCHNEEMANN, 81-64

LOS ALAMOS SCIENTIFIC LABORATORY
P.O. BOX 1663
LOS ALAMOS, NM 87544
ATTN GMX-6, J. W. TAYLOR

MARTIN MARIETTA AEROSPACE
ORLANDO DIVISION
P.O. BOX 5837
ORLANDO, FL 32805
ATTN M. C. GRIFFITH, LIB MP-30
ATTN W. W. MRAS, MP-413

MCDONNELL DOUGLAS CORPORATION
5301 BOLSA AVENUE
HUNTINGTON BEACH, CA 92647
ATTN STANLEY SCHNEIDER
ATTN W. OTAGURO
ATTN R. HARTMAN

NORTHROP CORPORATION
NORTHROP RESEARCH AND TECHNOLOGY CENTER
3401 WEST BROADWAY
HAWTHORNE, CA 92050
ATTN LIBRARY
ATTN DAVID N. POCOCK
ATTN ORLIE L. CURTIS
ATTN J. SROUR

MCDONNELL DOUGLAS ASTRONAUTICS COMPANY
HOLIDAY OFFICE CENTER
3322 MEMORIAL PARKWAY, S.W.
HUNTSVILLE, AL 35801
ATTN R. NICHOLS

MISSILE RESEARCH CORPORATION
P.O. DRAWER 719
SANTA BARBARA, CA 93102
ATTN ROY HENDRICK

PERKIN-ELMER CORPORATION
MAIN AVENUE
NORWALK, CT 06852
ATTN D. P. MATHUR, MS 218

THE RAND CORPORATION
1700 MAIN STREET
SANTA MONICA, CA 90406
ATTN H. LEIFER

RIVERSIDE RESEARCH INSTITUTE
80 WEST END AVENUE
NEW YORK, NY 10027
ATTN TOM LIBRARY

ROCKWELL INTERNATIONAL CORPORATION
AUTONETICS DIVISION
ELECTRO OPTICAL LABORATORY
P.O. BOX 4181
3370 MIRALOMA AVENUE
ANAHEIM, CA 92803
ATTN G. HOOVER
ATTN R. FLORENCE

SANTA BARBARA RESEARCH CENTER
75 COROMAR DRIVE
GOLETA, CA 93017
ATTN D. BODE
ATTN J. STEININGER

R&D ASSOCIATES
P.O. BOX 9695
MARINA DEL REY, CA 90291
ATTN S. CLAY ROGERS

RESEARCH TRIANGLE INSTITUTE
P.O. BOX 12194
RESEARCH TRIANGLE PARK, NC 27709
ATTN ENG. DIV, M. SIMONS

SCIENCE APPLICATIONS INC.
HUNTSVILLE DIVISION
2109 W. CLINTON AVENUE, #700
HUNTSVILLE, AL 35805
ATTN NOEL R. BYRN

TELEDYNE BROWN ENGINEERING COMPANY
RESEARCH PARK
300 SPARKMAN DRIVE
HUNTSVILLE, AL 35807
ATTN G. R. EZELL
ATTN G. EBERHART

HARRY DIAMOND LABORATORIES
ATTN MCGREGOR, THOMAS, COL, COMMANDING
OFFICER/FLYER, I.N./LANDIS, P.E./
SOMMER, H./OSWALD, R. B.
ATTN CARTER, W.W., DR., ACTING TECHNICAL
DIRECTOR/MARCUS, S.M.
ATTN KIMMEL, S., IO
ATTN CHIEF, 0021
ATTN CHIEF, 0022
ATTN CHIEF, LAB 100
ATTN CHIEF, LAB 200
ATTN CHIEF, LAB 300
ATTN CHIEF, LAB 400
ATTN CHIEF, LAB 500
ATTN CHIEF, LAB 600
ATTN CHIEF, DIV 700
ATTN CHIEF, DIV 800
ATTN CHIEF, LAB 900
ATTN CHIEF, LAB 1000
ATTN RECORD COPY, BR 041
ATTN HDL LIBRARY (3 COPIES)
ATTN CHAIRMAN, EDITORIAL COMMITTEE
ATTN CHIEF, 047
ATTN TECH REPORTS, 013

DISTRIBUTION (Cont'd)

HARRY DIAMOND LABORATORIES (Cont'd)

ATTN PATENT LAW BRANCH, 071
ATTN MCLAUGHLIN, P.W., 741
ATTN LANHAM, C., PROGRAM & PLANS OFFICE
ATTN WIMENITZ, F. N., 0024
ATTN GAUL, JAMES, 0024
ATTN BALICKI, FREDERIC, 0024
ATTN HALPIN, J., 280
ATTN REDDEN, M., 350
ATTN EISEN, H., 280
ATTN MCGARRITY, J., 280
ATTN WINOKUR, P., 280
ATTN BOESCH, E., 280
ATTN MCLEAN, B., 280
ATTN EPSTEIN, A., 280
ATTN SHARE, S. (15 COPIES)


F
6